Marine Geology, 86 (1989) 283–319
Elsevier Science Publishers B.V., Amsterdam — Printed in The Netherlands

SEDIMENTARY FACIES OF GLACIAL–INTERGLACIAL CYCLES IN THE NORWEGIAN SEA DURING THE LAST 350 ka

RÜDIGER HENRICH[1], HEIDEMARIE KASSENS[1], ELKE VOGELSANG[1] and JÖRN THIEDE[2]

[1]*Geologisch-Paläontologisches Institut Universität Kiel, Olshausenstrasse 40, D-2300 Kiel (F.R.G.)*
[2]*Geomar—Forschungszentrum für Marine Geowissenschaften, Wischhofstrasse 1–3, D-2300 Kiel (F.R.G.)*

(Received January 25, 1988; revised and accepted November 28, 1988)

Abstract

Henrich, R., Kassens, H., Vogelsang, E. and Thiede, J., 1989. Sedimentary facies of glacial–interglacial cycles in the Norwegian Sea during the last 350 ka. Mar. Geol., 86: 283–319.

Sediment fluxes were highest in the Norwegian Sea during late glacial/early deglacial periods, i.e., at oxygen isotope transition 4/3, below transition 6/5, at various levels within stage 6, and below stage 9. Dark diamictons deposited at these times reflect intense iceberg rafting in surface waters fed by surges along the front of the marine-based parts of the continental ice sheets in the southeastern sector of the Norwegian Sea. The high organic carbon content (0.5–1.3%) in these layers reflects input from erosion of terrigenious matter-rich sediments outcropping on the shelves. Partial oxidation of organic matter and decreased deep-water renewal may explain the strong carbonate dissolution observed during these periods. Interglacial environments were strongly variable throughout the last 350 ka. Circulation patterns of stage 5e best resemble modern conditions, while stage 7 and 9 sediments record a much weaker Norwegian Current.

Introduction

Facies changes in pelagic upper Quaternary Norwegian Sea sediments

The Norwegian–Greenland Sea has been strongly influenced by repetitive growth and decay of continental ice sheets over Greenland and Scandinavia and by migration of the oceanic Polar Front. Sedimentary records from this area are therefore well located to study glacial–interglacial climatic shifts and changes in ocean circulation patterns.

The two main surface current systems in the Norwegian–Greenland Sea are the inflow of warm saline North Atlantic Surface Water (NAW) between the Shetland and the Faroe Islands (Norwegian Current) and the inflow of cold polar surface water and sea ice through the Fram Strait (East Greenland Current). The warm saline Norwegian Current follows the Norwegian continental margin and divides near Bear Island into two branches, one of which is deflected onto the Barents shelf. The other branch continues north of Svalbard and into the Arctic Ocean under the pack-ice cover. The East Greenland Current occupies a broad area along the eastern margin of Greenland and exits the Norwegian–Greenland Sea through the Denmark Strait (Fig.1a). Between these two major current systems, a wide area in the centre of the Greenland Sea and Iceland Sea is occupied by a mixed surface water layer called Arctic Surface Water (ASW). This water mass has lower salinity compared to NAW and is colder, although it has strong temperature variations (Johannessen, 1986). The oceanic Polar Front, broadly defined as the boundary between Atlantic and Arctic water, is located in this region.

0025-3227/89/$03.50

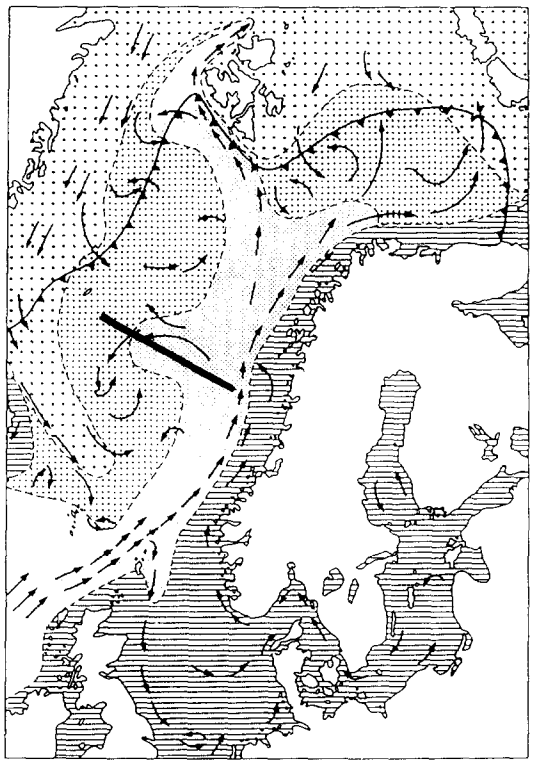

Fig.1.a. Map showing the surface waters and the main circulation pattern in the Norwegian Sea and adjoining seas. 1 = Arctic water; 2 = mixing water; 3 = Atlantic water (water in the Norwegian Current); 4 = coastal, Baltic and North Sea water (water in the Norwegian Coastal Current); 5 = surface currents; 6 = sea-ice boundary in April. Position of investigated core transect is indicated by the heavy line. Modified from Mosby (1968) and Hald and Vorren (1987). b. Regional setting of the core transect.

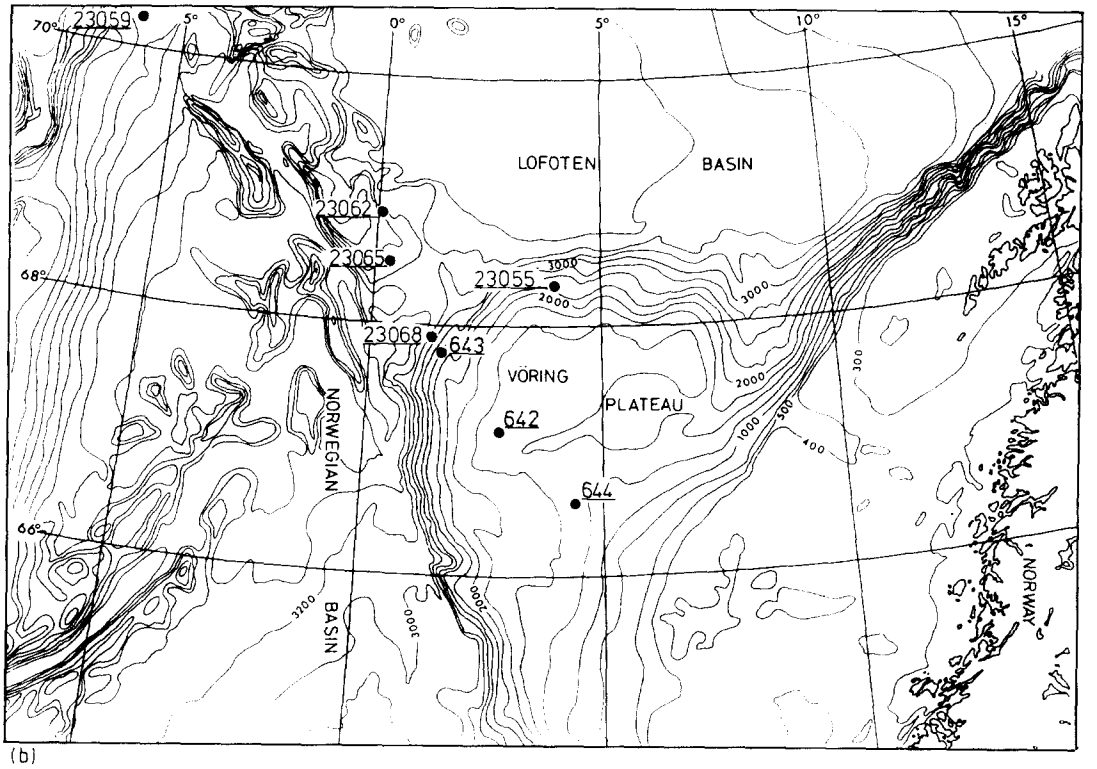

(b)

Surface sediments on the floor of the Norwegian–Greenland Sea reflect the major surface water circulation pattern (Gorshkova, 1960; Kellogg, 1975). High carbonate shell productivity, e.g., high contents of planktonic foraminifers and coccolithophorids, are found under the Norwegian Current. Higher amounts of the relatively warm-water species, e.g., right-coiling *Neogloboquadrina pachyderma* and other subpolar species, reflect the warm environment provided by the Norwegian Current system. Coastal areas off Norway and Greenland are dominated by terrigenous clays and sands winnowed of the fine fraction by bottom-current activity. Most of the shelf sediments consist of relict Pleistocene material deposited by ice rafting or as till (Holtedahl, 1959; Vorren et al., 1984). Little or no ice-rafted debris, but commonly foraminiferal clays are observed in a zone west of Svalbard and in a zone south of Svalbard towards Greenland, areas which today are covered by winter sea-ice.

At high latitudes between Svalbard and Jan Mayen ASW locally becomes so dense owing to surface cooling that it sinks and fills the abyss of the Norwegian–Greenland Sea. During winter, regional overturning of dense surface water and less dense deep water in the Iceland Sea and Greenland Sea may result in deep or intermediate convection and contribute to deep-water formation (Johannessen, 1986; Swift, 1986). Additionally, dense water formed on the Barents shelf in winter during sea-ice formation flows down the continental slope along the Bear Island Trough (Sarynina, 1972). Newly formed deep water leaves the Norwegian–Greenland Sea through the Denmark Strait and over sills between Iceland and the Shetland Islands, contributing to North Atlantic Deep Water (NADW) (Worthington, 1970; Meincke, 1983).

Glacial environments have been reconstructed, based on sedimentological and stable isotopic data combined with faunal abundances and their compositional differences, by Kellogg (1975, 1976, 1977), Kellogg et al. (1978). Belanger (1982) and Streeter et al. (1982). In a synthesis study, Kellogg (1980) provided various synoptic charts covering the entire Norwegian–Greenland Sea, including sea-surface temperature distribution (calculated from temperature transfer functions; Imbrie and Kipp 1971). The essentials of these charts are as follows:

During the last glacial maximum, at 18 ka, the Norwegian–Greenland Sea remained permanently covered by sea ice. Ice circulated in a single sluggish cyclonic gyre. During stage 5a, the transition from the last interglacial to the last glacial at about 82 ka, a weak two-gyre system is proposed. Most of the Norwegian Sea is shown to be permanently ice-covered except for a narrow region with seasonal ice in the central parts. The reconstruction for the last interglacial maximum (stage 5e, 124–115 ka) appears to show a surface circulation similar to, but stronger than that prevailing today. This type of environment is thought to have never been established again during the last 450 ka.

A modified view was presented by Belanger (1982) who suggested the existence of warm, productive subpolar waters throughout isotope stages 1 and 5 and parts of 4, based on combined coccolith, benthic and planktonic foraminifer evidence. Productivity is thought to have been considerably lower during stages 2 and 3, which was interpreted to be consistent with year-round ice cover.

Streeter et al. (1982) showed that the glacial Norwegian Sea could not have been a sink for dense surface water, and thus not a source of deep-water overflow in the last 130 ka. Their evidence for this conclusion was the benthic foraminifer faunas and oxygen isotope stratigraphy which indicated bottom waters warmer than those occurring today.

It is the purpose of this study to test and modify the existing palaeo-oceanographic models by a new methodological approach based on a combined facies analysis. Deep-sea sediment facies are defined by sedimentological (sedimentary structures, grain-size analysis, carbonate contents and dissolution records, content and quality of organic carbon, and coarse-component content and composi-

tion), micropalaeontological (benthic and planktonic faunal assemblages) and early diagenetic properties. Flux rates of bulk sediment and various components are determined in order to quantify important oceanographic parameters such as carbonate shell production in surface waters and input of coarse ice-rafted debris. Typical lithofacies successions and variations in flux rates in time and space are interpreted in conceptual models and are discussed in the context of the palaeo-oceanographic evolution of the Norwegian Sea during the past 350 ka.

Regional setting of cores

The new R.V. *Meteor* recovered a number of undisturbed, high-quality, long kasten cores (900 cm^2 basal area; Kögler, 1963) along a transect from the Vøring Plateau to Jan Mayen (*Meteor* cruise 2/2; Gerlach et al., 1986). The profile (Fig.1b) is located just north of the Jan Mayen Fracture Zone, crossing the tops and flanks of various seamounts and submarine plateaus (for locations and water depths of cores see Figs.1b and 4, and Table 1). The Vøring Plateau is a prominent feature of the Norwegian continental margin (Fig.1b). It is a marginal high with an almost flat surface at a water depth of about 1400 m., bordered by a region of shallower elevation (water depth 1280 m). The plateau is bordered by the Norwegian shelf (200–400 m deep) to the east, the Lofoten Basin (about 3000 m deep) to the north and west, and the Norwegian Basin to the south (about 2500 m deep) (Fig.1).

The main surface water masses influencing the study area are the warm Atlantic water of the Norwegian Current over the Vøring Plateau and the central sector, and the colder Arctic Surface Water in the western sector of the profile.

Methods

Sampling

Sampling, visual description and photographing of cores were carried out on board R.V. *Meteor*. Cores were sampled at an average spacing of 5 to 10 cm, equivalent to a time span of 1–5 ka depending on the sedimentation rate. Additional samples were collected when changes in lithology were observed during visual core description. Sample sizes were 100 cm^3.

Continuous slabs of sediment 0.8 cm thick were taken throughout the core for X-ray radiography. Handling procedures are summarized in a flow diagram (Fig.2). About 3–5 cm^3 of each sample were separated for bulk carbonate, organic carbon and major element (e.g., Fe and Mn) measurements. The remainder was disintegrated in a 10–20% ammonia-buffered hydrogen peroxide solution and wet-sieved on a 63-μm sieve. The residue was retained, dried and weighed. The >63-μm fraction was also dried, weighed and dry-sieved into the following fractions: 63–125 μm, 125–250 μm, 250–500 μm, 500–1000 μm and >1000 μm. The weights of individual fractions and the weight loss during sieving were determined. Weight losses were generally less than 0.5%.

TABLE 1

Position and water depth of long box cores investigated

No.	Latitude (°N)	Longitude (°E)	Water depth (m)	Recovered section (m)	Penetration (m)
23055-3	68.25.4	04.01.3	2311	6.67	6.77
23059-3	70.18.3	03.07.4	2281	6.22	7.05
23062-1	68.43.7	00.10.1	2244	7.00	7.00
23065-1	68.29.7	00.49.1	2802	7.85	7.85
23068-1	67.50.0	01.30.3	2230	7.60	8.50

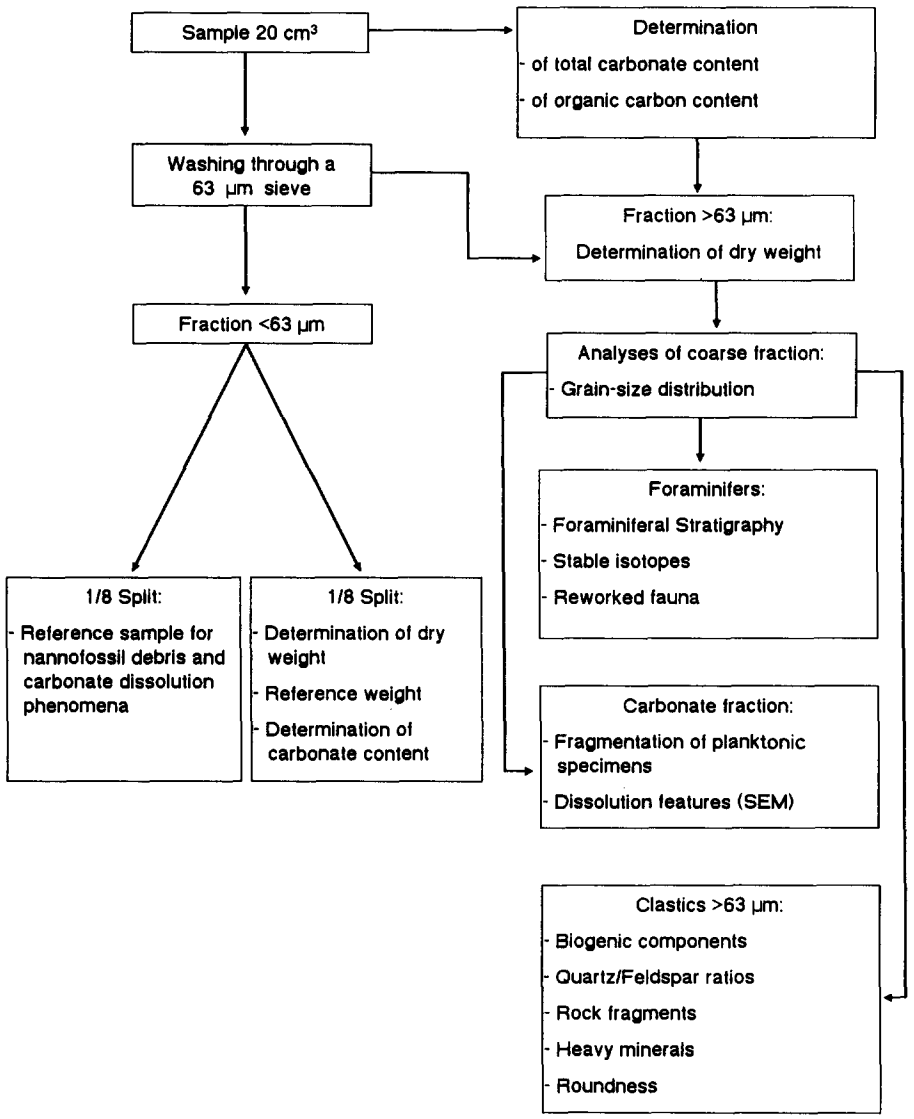

Fig.2. Flow diagram of sample processing in the sedimentology laboratory.

Physical properties

Additional samples spaced at 5–10 cm intervals for determination of physical properties were taken by means of special metal cylinders (10 cm^3) immediately after recovery of the cores. Samples were protected against desiccation and shipped to the laboratory onshore. Weight was measured before and after drying for 15 h at 105°C and subsequent cooling in a desiccator for at least 2 h in order to determine wet and dry density, and water content. Dry bulk density is defined as the mass of solids related to the total volume of the sample. Physical property data were applied in calculations of accumulation rates.

Carbonate, organic carbon and elemental analysis

Bulk carbonate and organic carbon contents were determined on all samples. Additionally, carbonate contents from all samples of the <63-µm fraction in cores 23059, 23062, 23065

and 23055 were determined. Measured weight percentages of fine-fraction carbonate were corrected for the total amount of the <63-μm fraction, and the percentage of coarse-fraction carbonate was calculated using the following equation:

$$\% \ CaCO_3(>63\ \mu m)^* = \% \ CaCO_3(\text{bulk}) - \% \ CaCO_3(<63\ \mu m) \times \%(<63\ \mu m)/100$$

Measurements were carried out with an infrared gas analyser. This instrument is based on photometric determination, utilizing infrared absorption of CO_2 released from a sample after extraction of carbonate in phosphoric acid. The standard deviation is less than 0.1% for both carbon and carbonate values.

Elemental composition of bulk sediments, e.g., Fe and Mn contents, were measured with an atomic absorption spectroscopy analyzer after extraction in perchloric acid.

Coarse-fraction and grain-size analysis

About 500–700 grains from a representative sample split of the 125–500 μm fraction were counted and the predominant biogenic, terrigenous and authigenic components were distinguished (see Sarnthein, 1971). The 125–500 μm fraction was chosen because results should be comparable to counts from micropalaeontological studies. Data of this subfraction may best represent the major changes in biogenic and terrigenous coarse-fraction components. Grain counts were corrected for the percentage of coarse fraction of the bulk sample in order to measure downcore changes on the same scale.

SEM dissolution studies on Neogloboquadrina pachyderma

Most parameters commonly used for dissolution studies in low- and mid-latitude oceans cannot be applied to polar and subpolar sediments because of the large variations in ecological conditions from glacial to interglacial stages in both surface- and bottom-water environments. Moreover, the high-latitude pelagic sediments, like those in other regions, are affected by variable dilution from non-carbonate and reworked-carbonate sources, e.g., terrigenous ice-rafted debris and resuspended ancient carbonate and mud from the shelf. Thus, the equation established by Berger (1971) to determine weight loss of carbonate during dissolution cannot be applied to this sedimentary environment because it relies on a constant input of non-carbonate sources. Benthic foraminiferal associations react sensitively to changes in deep-water oceanography (Belanger and Streeter, 1980; Belanger, 1982; Streeter et al., 1982; Sejrup et al., 1984). Consequently, the planktonic/benthic ratio is also inadequate in indicating dissolution. Large-scale differences in dissolution susceptibility of various species of planktonic foraminifers are frequently used to establish dissolution rates (Berger, 1968; Crowley, 1983). Glacial planktonic foraminifer associations in high latitudes, however, have only a monospecific composition, with left-coiling *N. pachyderma*. This is the only species which occurs in both glacial and interglacial sediments. We suggest that dissolution can be recorded by conventional fragmentation indices of this species and by sensitive SEM-based dissolution indices (Henrich, 1986).

The SEM approach is based on recognition of four stages of structural breakdown during progressive dissolution of the two morphotypes of *N. pachyderma*. In particular, the microcrystalline ultrastructure of reticulate forms and the coarse crystalline ultrastructure of crystalline forms with development of a typical secondary calcified crust are distinguished (for details of the skeletal ultrastructure and mode of chamber formation see Kennett and Srinivasan (1980), Henrich (1986). Sediment traps in the northern Pacific showed seasonal variations in the flux of crystalline and reticulate forms, indicating that the crystalline form is adapted to waters colder than 8°C (Reynolds and Thunell, 1986).

Successive stages in dissolution are listed in Table 2 and displayed in Plates 1 and 2. In many instances, tests from a transition between the two end members, typically with the

*Corrected for percentage on bulk sediment weight.

TABLE 2

Characteristic ultrastructural changes during progressive dissolution of *N. pachyderma* sin. (SEM-defined dissolution indices)

Dissolution index	Indicative changes in ultrastructure of the tests
$D_{0A,B}$	Unaffected reticulate or crystalline tests
D_{1A}	Incipient dissolution of reticulations, preferentially affecting chamber sutures and and pores of the outermost chambers. Dissolution of the innermost primary calcitized wall occurs simultaneously
D_{2A}	Selective removal of residual ridges with granular calcite platelets. Often together with formation of small superficial dissolution holes and cavities.
D_{3A}	Strong dissolution and incipient fragmentation often induced and enhanced by strong dissolution from the inner chamber walls. Steep corrosion relief on the test surfaces
D_{1B}	Incipient dissolution of the coarse scalenohedra fabric with typical flame structures on the crystal surfaces as well as preferential dissolution along the rims of the crystals. Advanced substages of D-I_B reveal irregular ablation and corrosion on crystal surfaces
D_{2B}	Corroded scalenohedra from all sites strongly associated with loosening of the densely packed fabric of prisms. In this preservation stage, parts of the test can easily be removed by weak currents. Often, this stage is additionally characterized by deep holes in the chamber walls and/or by fracturing of weakened chambers
D_{3B}	Ghost structures of scalenohedra with very intense corrosion of crystals. The almost-intact test morphology can easily be destroyed by any weak attack. Frequently, partial removal of crystals is observed
$D_{4A,B}$	Final stage of corrosion. Complete disintegration of test into strongly corroded fragments

A—reticulate form of *N. pachyderma* sin.; B—crystalline form of *N. pachyderma* sin.
Note: *N. pachyderma* form *A* often transforms its test during ontogeneses. In sediment samples, often many transitional reticulate and crystalline forms are observed. In these cases, dissolution indices should only be identified on typically developed chambers.

youngest chamber still reticulate while the older chambers are converted to the crystalline morphostructure. In these cases, the most characteristically developed chambers were chosen for the determination of the SEM dissolution index in order to avoid confusion with transformation processes in the crust. Samples were processed for SEM investigations in the following way:

(1) Splitting of the sample with a microprobe splitter to an aliquot containing about 40–50 tests.

(2) Mounting of the tests onto a SEM carrier.

(3) Determination in the SEM of the degree of dissolution in each test and conversion of the dissolution steps into a numerical index.

(4) Calculation of a composite numerical dissolution index for each sample.

Dissolution susceptibility for the reticulate and crystalline morphotypes may differ slightly, as discussed by Henrich (1986). However, the magnitude of this difference still has to be evaluated by *in-situ* dissolution experiments in the ocean similar to those carried out by Henrich and Wefer (1986) for shallow-water particles. Hence, the various steps of dissolution in this study are assumed to be equal for reticulate and crystalline forms. A composite numerical dissolution index can then be calculated using the following equation:

$$D_{A,B} = (D_{0A,B} \times n_1 + D_{1A,B} \times n_2 + D_{2A,B} \times n_3 + D_{3A,B} \times n_4)/(n_1 + n_2 + n_3 + n_4)$$

where $D_{A,B}$ = composite numerical dissolution index for the reticulate (A) and crystalline (B) morphotype of *N. pachyderma* sin.,
$D_0 \ldots D_3$ = steps of dissolution (see Table 2; 0 = unaffected, 3 = strong dissolution),
and $n_1 \ldots n_4$ = number of tests, with dissolution index subscript.

PLATE 1

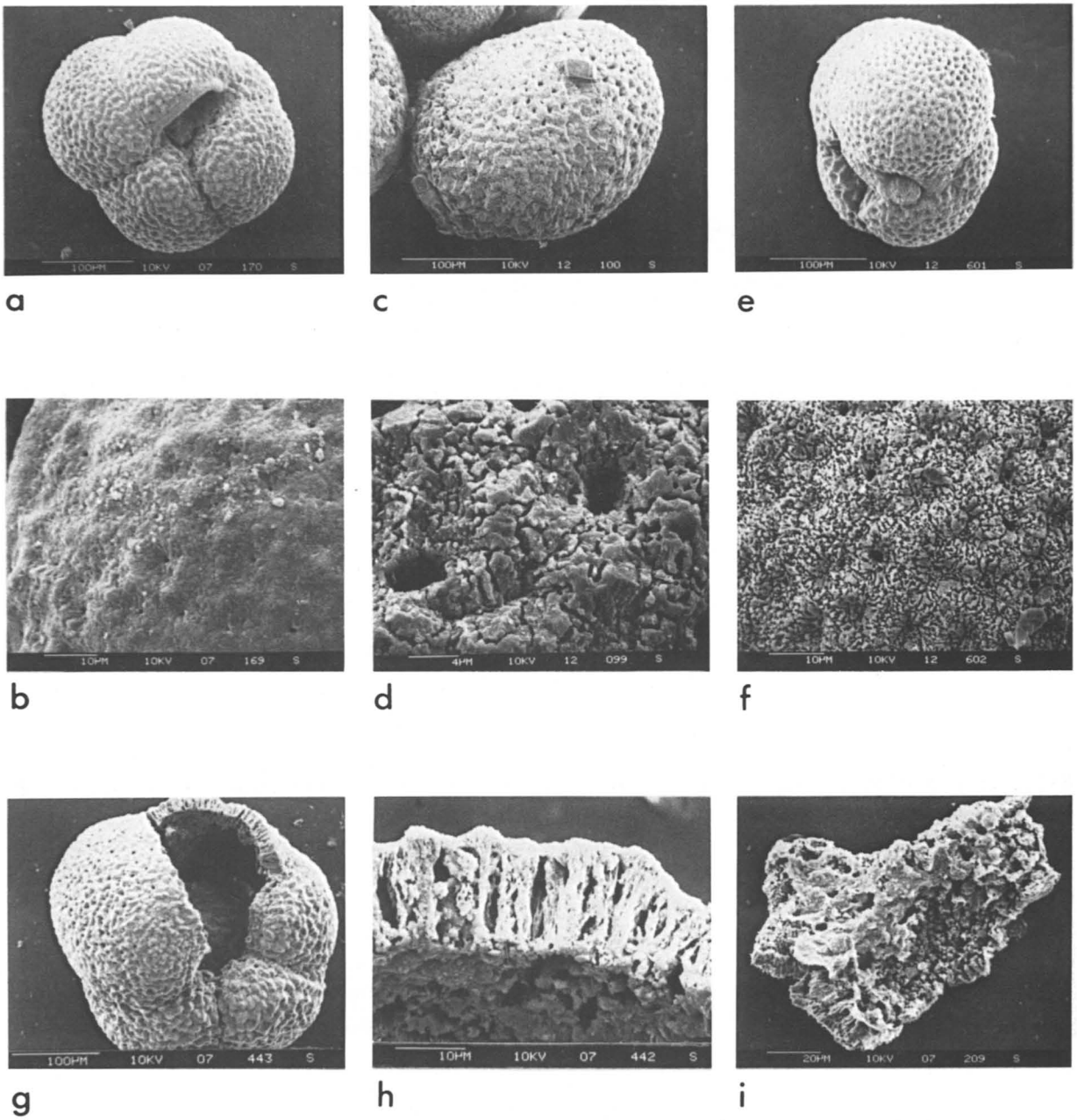

SEM dissolution indices on *N. pachyderma* sin., reticulate morphotype. a and b. Well-preserved reticulate test (D_{0A}). c and d. Incipient dissolution at the surface of the test (D_{1A}). e and f. Strong dissolution at the surface of the test (D_{2A}). g and h. Strong dissolution starting from the interior parts of the test resulting in fragmentation (D_{3A}). i. Extremely corroded fragment (D_{4A}).

PLATE 2

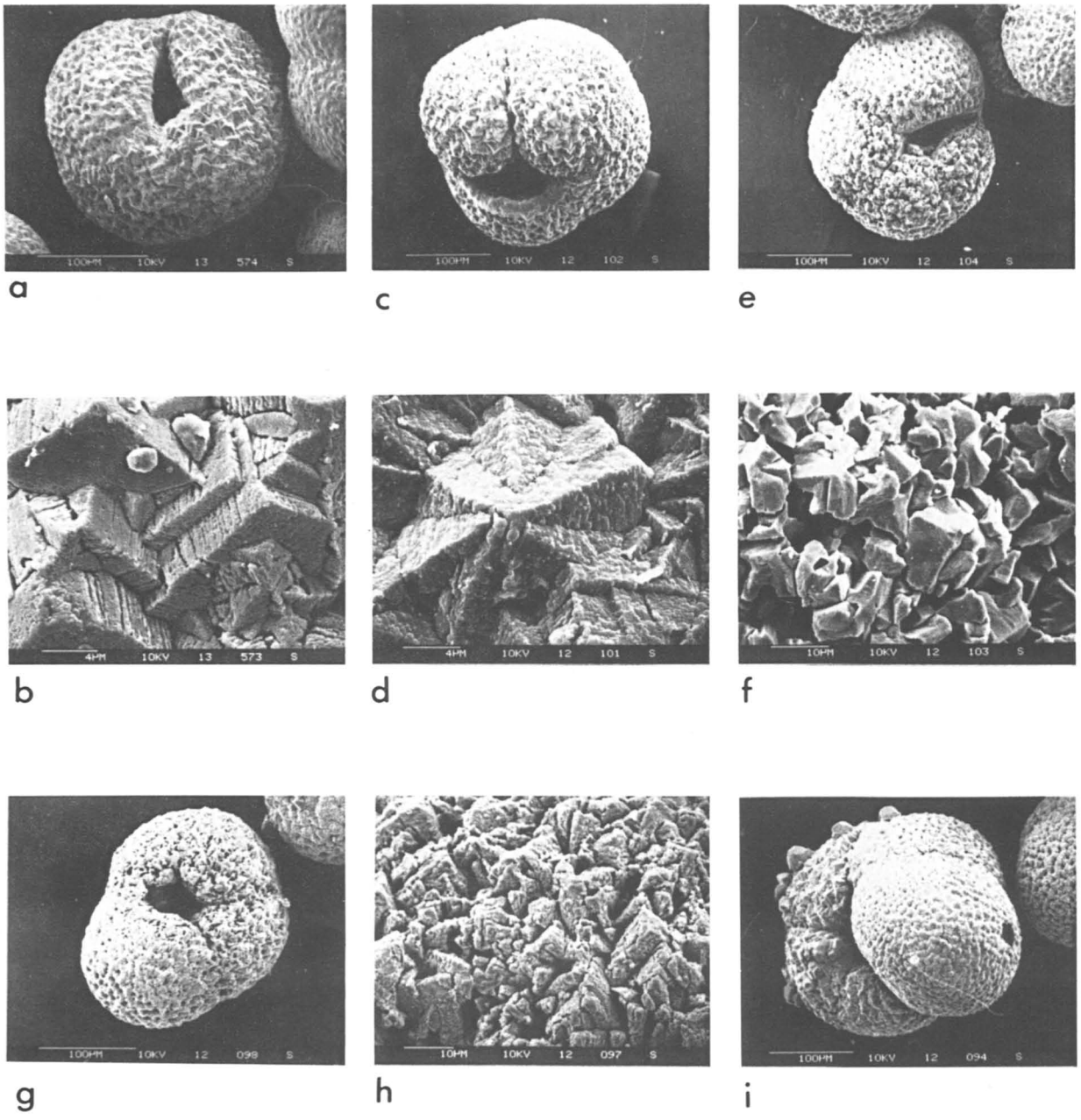

SEM dissolution indices on *N. pachyderma* sin., crystalline morphotype. a and b. Initial dissolution reflecting typical corrosion relief on the surface of the rhombohedra (D_{1B}). c and d. Initial dissolution on rosette-like rhombohedra aggregate revealing irregular dissolution relief (D_{1B}). e and f. Intermediate dissolution showing strong corrosion of rhombohedra and loosening of the framework of the crystal (D_{2B}). g and h. Strong dissolution with extreme corrosion of rhombohedra and strong loosening of the framework of the crystal (D_{3B}). i. Crystalline morphotype, youngest chamber still reflecting fine crystalline reticulations; overgrowth of authigenic carbonate cements.

Oxygen isotope stratigraphy, sedimentation rates and accumulation rates

Biostratigraphy in glacial–interglacial cycles of polar environments is of limited use, because endemic and persistent faunal and floral assemblages predominate. Where sufficient foraminifers can be found, oxygen isotope profiles provide a high-resolution stratigraphy for Norwegian Sea sediments.

Oxygen and carbon isotope measurements on the planktonic foraminifer *N. pachyderma* sin. (125–250 μm fraction) were performed in the ^{14}C Laboratory of the Institute of Nuclear Physics at Kiel University on the Carbo-Kiel equipment connected to a Finnigan MAT 251 mass spectrometer.

Stage boundaries were established in the oxygen isotope records. Isotope events (Imbrie et al., 1984; Martinson et al., 1987) and curve shapes were compared with published isotope records. In addition, sedimentological features in the cores, such as the position of volcanic ash beds and carbonate records, were considered.

The oxygen isotope stratigraphy permitted calculation of linear sedimentation rates (LSR) using the absolute age determinations established for isotope stages in the SPECMAP time scale (Imbrie et al., 1984; Martinson et al., 1987). In addition, stage 1/2 and stage 2/3 boundaries were calculated as 15 ka and 27 ka, respectively (Bard et al., 1987, Sarnthein et al., 1988). All age determinations are listed in Table 3. Bulk accumulation rates and accumulation rates for various other sedimentological parameters were determined based on the method of Thiede et al. (1982).

Results

Time stratigraphic control

Stratigraphic control is based mainly on the oxygen and carbon isotope records (cores 23059, 23062, 23065, 23068 and 23055). Recognized stage boundaries and isotopic events are indicated in Fig.3 (Vogelsang, Unpubl.). The exact position of some stage boundaries is occasionally somewhat blurred by interruptions in the isotopic records caused by strong carbonate dissolution (Figs.10 and 15). Isotopic data based on the few tests of foraminifers left in these specific horizons must be considered with caution because of bioturbation. Isotopic boundaries will be displaced towards the foraminifer-free core sections because of the gradient in test frequency (Hutson, 1980; Duplessy et al., 1986). Records of cores 23059 and 23062 reflect isotope stages 1–9 and substages comparable to previously published records from the Norwegian–Greenland Sea (Kellogg et al., 1978; Kellogg, 1980; Labeyrie and Duplessy, 1985).

Additional stratigraphic information is provided by the $\delta^{13}C$ records of *N. pachyderma*. The stratigraphic value of these records was first recognized by Labeyrie and Duplessy (1985). They reported three clear $\delta^{13}C$ transitions in Norwegian Sea cores covering the past 140 ka, which are simultaneous with oxygen isotopic transitions 6/5, 5/4 and 2/1. Our records (Vogelsang, Unpubl.) confirm these results and permit extension of the $\delta^{13}C$ scale back to about 350 ka.

Glacial–interglacial lithofacies types

The most prominent features of glacial–interglacial cycles in the Norwegian Sea are pronounced changes between light and dark sediment layers. They appear on a large scale (metres) and on a smaller scale (centimetres to tens of centimetres) (see Eldholm et al., 1987; Henrich, 1989). Light layers are usually thicker than dark layers and display three major lithofacies types.

Facies A consists of predominantly brownish to dark brownish foraminiferal muds and foram–nanno oozes with high carbonate (30–60%) and foraminifer (30–40%) contents, and low amounts of organic carbon (0.1–0.3%) and coarse terrigenous debris (mostly less than 5%). Bioturbation features, both as indistinct and well-developed burrows, are the most commonly observed sedimentary structures. The

TABLE 3

Age–depth determinations and linear sedimentation rates

Stage transition	Age (ka)	Depth (cm)	Difference (cm)	Difference (ka)	LSR (cm/ka)	Stage
23055-3						
1/2	12	40	40	12	3.33	1
2/3	27	104	64	15	4.23	2
3/4	59	205	101	35	2.86	3
4/5	71	235	30	12	2.50	4
5/6	128	321	86	57	1.51	5
6/7	186	600	279	58	4.81	6
23068-3						
1/2	12	41	41	12	3.42	1
2/3	27	132	91	15	6.07	2
3/4	59	255	123	32	3.84	3
4/5	71	276	21	12	1.75	4
5/6	128	412	136	57	2.39	5
6/7	186	780	368	58	6.34	6
23065-3						
1/2	12	22	22	12	1.83	1
2/3	27	65	43	15	2.87	2
3/4	59	160	95	32	2.97	3
4/5	71	174	14	12	1.17	4
5/6	128	280	106	57	1.86	5
6/7	186	485	205	58	3.53	6
7/8	245	535	50	59	0.85	7
8/9	303	640	105	58	1.81	8
9/10	339	670	30	36	0.83	9
23062-1						
1/2	12	25	25	12	2.08	1
2/3	27	70	45	15	3.00	2
3/4	59	155	85	32	2.66	3
4/5	71	166	11	12	0.92	4
5/6	128	254	88	57	1.54	5
6/7	186	460	206	58	3.55	6
7/8	245	535	75	59	1.27	7
8/9	303	620	85	58	1.47	8
9/10	339	635	15	36	0.42	9
23059-3						
1/2	12	30	30	12	2.50	1
2/3	27	77	47	15	3.13	2
3/4	59	155	78	32	2.44	3
4/5	71	170	15	12	1.25	4
5/6	128	230	60	57	1.05	5
6/7	186	360	130	58	2.24	6
7/8	245	425	65	59	1.10	7
8/9	303	495	70	58	1.21	8

variety of bioturbation features includes centimetre-sized burrow tubes of the *Planolithes* type, millimetre-sized and up to 20 cm long vertical tubes, and close networks of thin-banded tube burrows of the genera *Mycellia sensu* Blampeded and Bellaiche (Figs.4–8). Lithofacies A was deposited during interglacials.

Facies B consists of silty muds and sandy

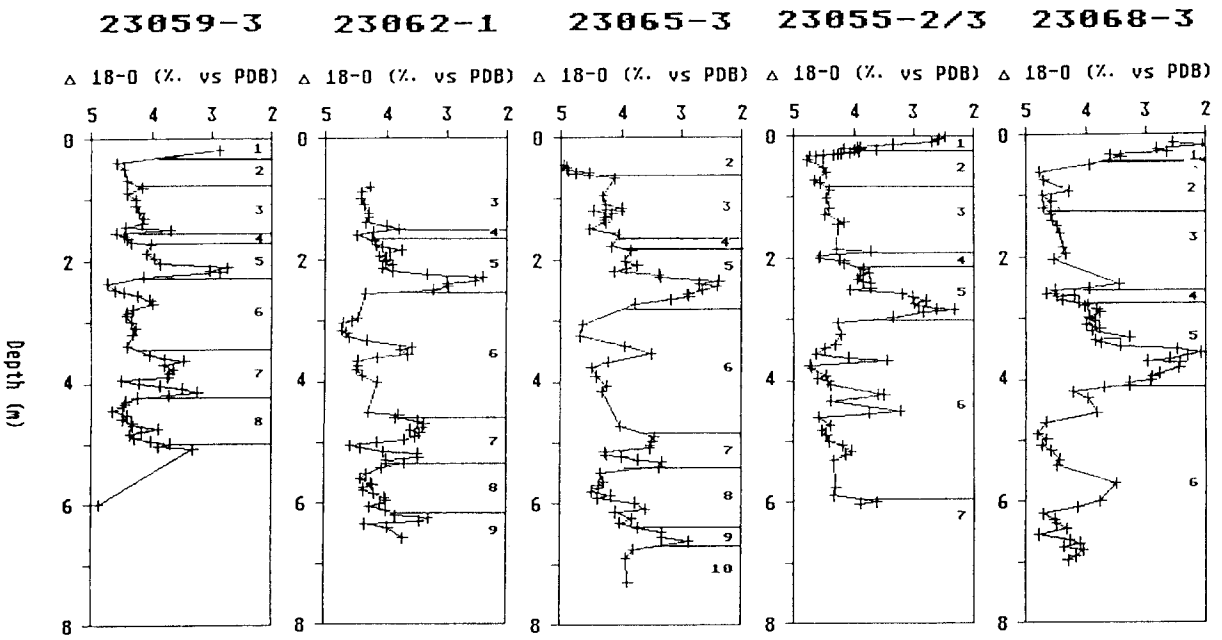

Fig.3. Oxygen isotope records (23059, 23062, 23065, 23055 and 23068) measured on left-coiling *N. pachyderma* sin.; size fraction 125–250 μm.

muds with the same colour and bioturbation features as facies A, but with lower carbonate (1–10%) and foraminifer (1–10%) contents and low to moderate organic carbon values (0.2–0.3%). Coarse terrigenous material is enriched, often within distinct layers. Occasional coarse lithic dropstones and some dark olive grey mudclasts are observed (Figs.4–9). Sediments of type B accumulated during early and late interglacial periods as well as during glacial periods.

Facies C consists of grey to dark grey silty muds, with low carbonate (generally 1–5%, seldom up to 10%) and foraminifer (1–5%) contents, moderate organic carbon contents (0.2–0.4%), moderate amounts of coarse sand-sized terrigenous debris (5–10%), scattered dropstones, and a few mud clasts. Bioturbation features similar to those in facies A may be present, but without thorough homogenization of the sediment. Facies C forms the normal background sediment in the colour cycles on the large scale where thick beds of facies C alternate with thin horizons of facies A and B (Figs.4–9). Facies C records the sedimentary environment of glacial periods.

Three major types of dark lithofacies are intercalated in these light sediment packages. These were either deposited during the major transitions from a glacial to an interglacial stage or within a glacial period with a very specific oceanographic configuration.

Facies D consists of very dark grey to black sandy to silty muds with very low contents of carbonate (0–0.3%) and foraminifers (commonly less than 50 tests) and high percentages of organic carbon (0.5–1.2%). Commonly, these

Fig.4. Lithofacies distribution along the transect Vøring Plateau–Jan Mayen. Determinations of oxygen isotope stage boundaries at the corresponding subbottom depth levels are indicated with arrows. Dark lines display isochronous lithological correlations along the transect. Note occurrence of volcanic ash layer within stage 8 and the E–W transitions of facies types F, D and E into facies types B and C.

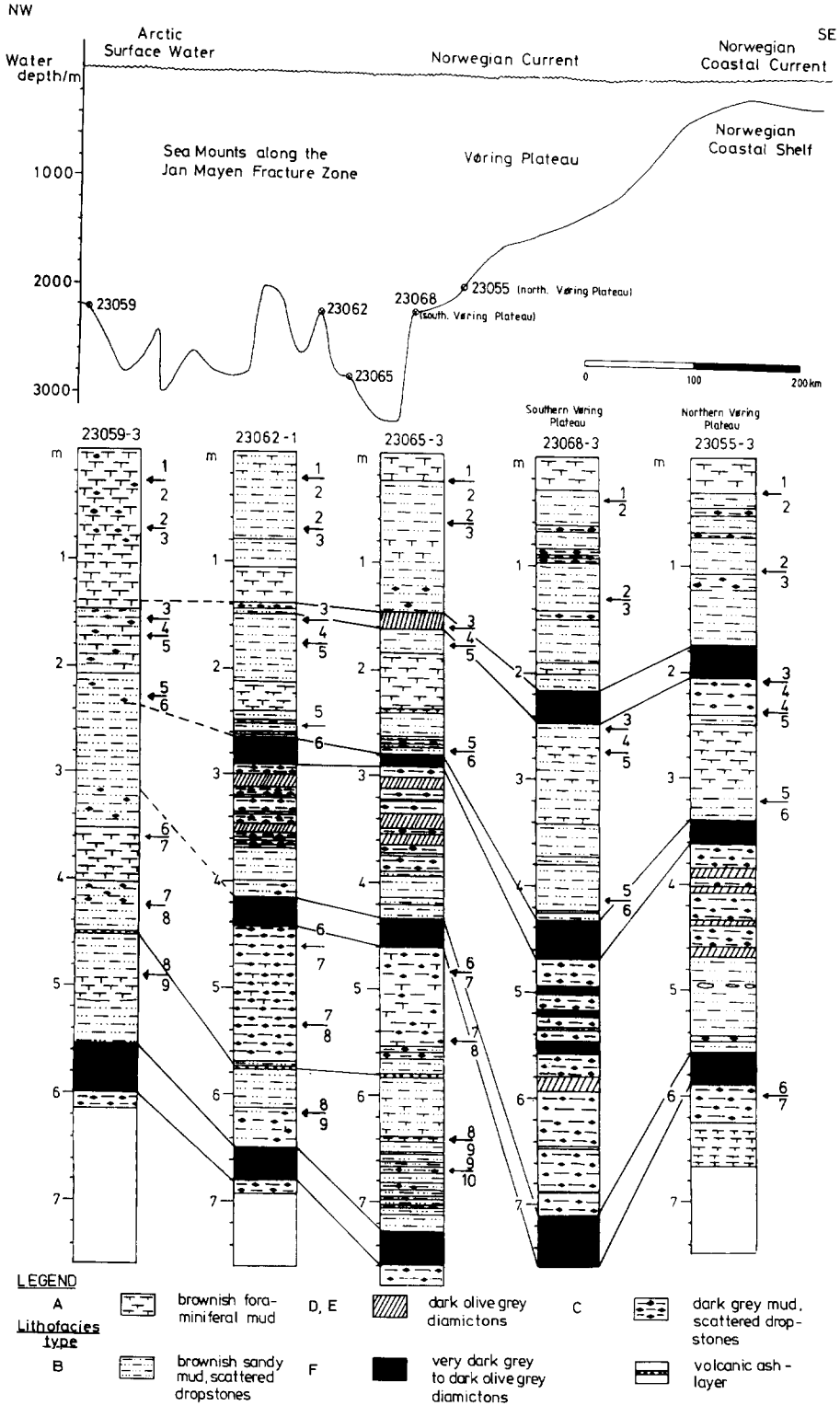
NW
SE
Water depth/m
Arctic Surface Water
Norwegian Current
Norwegian Coastal Current
Sea Mounts along the Jan Mayen Fracture Zone
Vøring Plateau
Norwegian Coastal Shelf
1000
2000
3000
23059
23062
23065
23068
23055 (north. Vøring Plateau)
(south. Vøring Plateau)
0
100
200km
Southern Vøring Plateau
Northern Vøring Plateau
23059-3
23062-1
23065-3
23068-3
23055-3
m
LEGEND
Lithofacies type
A
brownish foraminiferal mud
B
brownish sandy mud, scattered dropstones
D, E
dark olive grey diamictons
F
very dark grey to dark olive grey diamictons
C
dark grey mud, scattered dropstones
volcanic ash-layer

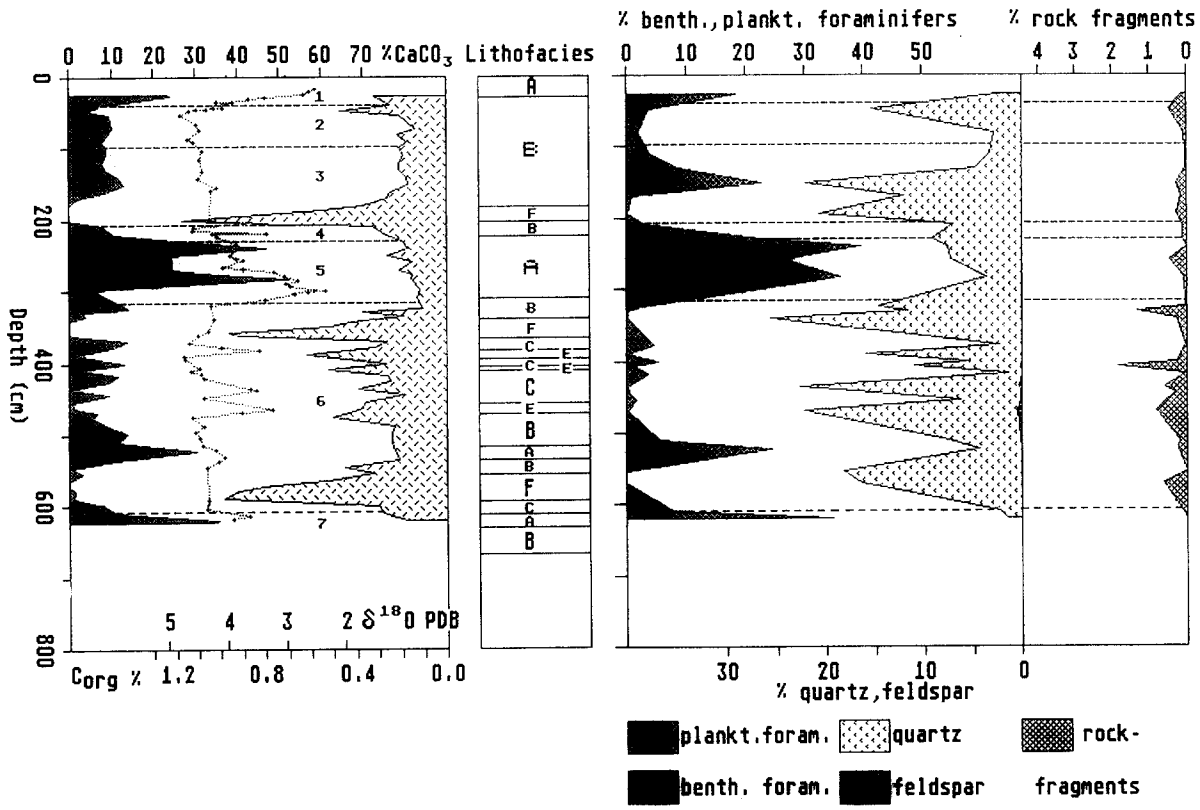

Fig.5. Basic sedimentology and oxygen isotope stratigraphy of core 23055-3. Note strong anticorrelation of bulk carbonate versus organic carbon weight percentages, and anticorrelation of planktonic/benthonic foraminifer versus quartz/rock fragment contents.

layers contain large amounts of sand-sized terrigenous debris (20–30%), as well as densely scattered dropstones and abundant mud clasts. Due to the absence of bioturbation these horizons are characterized by a sharp base and top (Figs.4–9).

Facies E is composed of dark olive grey sandy muds with very low carbonate (0–0.3%) and foraminiferal contents (commonly less than 50 tests), high organic carbon content (0.5–1.2%), densely scattered dropstones, and abundant mud clasts (Figs.4–9). These layers commonly have a sharp top and base but sometimes contacts are blurred by bioturbation (compare Fig.9b).

Facies F forms a complex layer consisting of a basal, very dark grey to black sandy mud with numerous scattered dropstones and common large mud clasts. It grades upward into a dark olive grey sandy mud with abundant dropstones and mud clasts. The entire package is very low in carbonate (0–0.3%) but high in organic carbon (0.5–1.2%). In higher parts of F-facies sections, sedimentary structures, especially the mud clasts, may be truncated by brownish iron lamination, spaced at intervals of a few millimetres to a few centimetres (Fig.9a). These diagenetic laminations in turn may be truncated by younger burrows filled with sediment from above. The laminated horizons reveal a remarkably higher degree of consolidation and lithification compared to the sediments above and below (Kassens, Unpubl.). In most cases, facies F is succeeded by sediments of lithofacies B, and occasionally by lithofacies C. An illustration of lithofacies

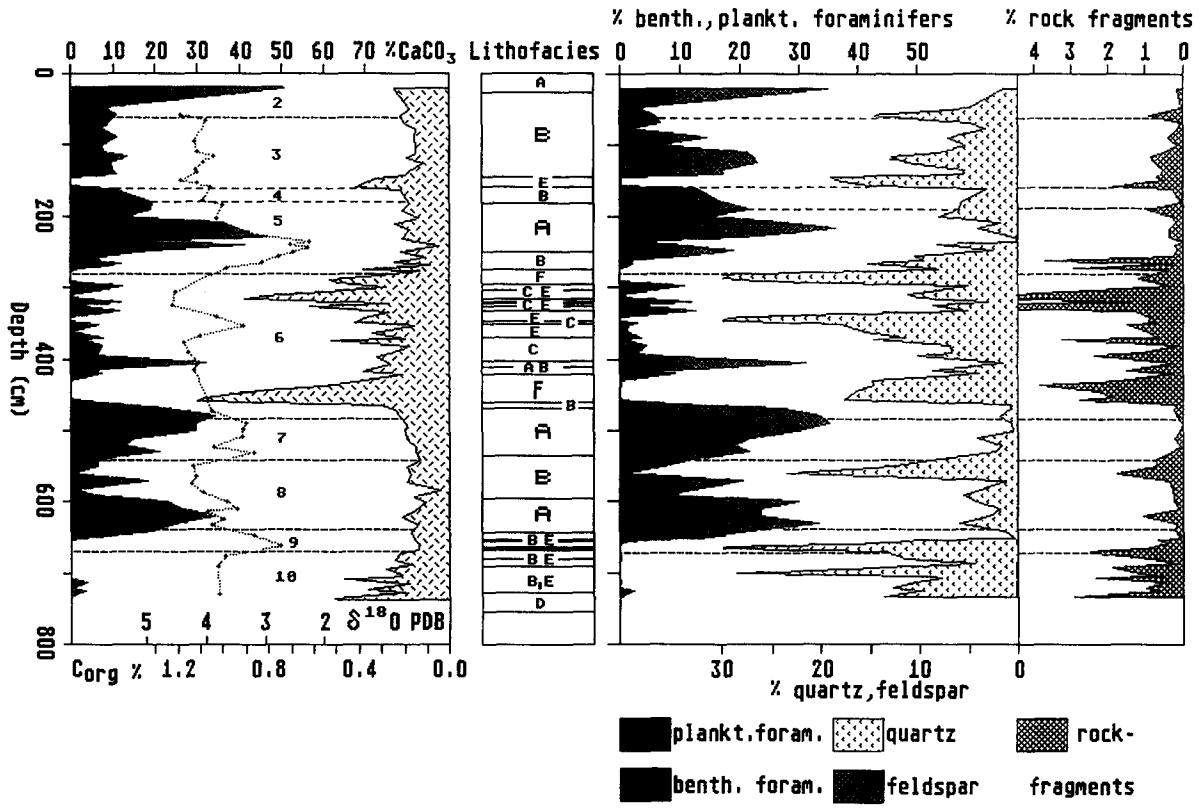

Fig.6. Basic sedimentology and oxygen isotope stratigraphy of core 23065-3. Note strong anticorrelation of bulk carbonate versus organic carbon weight percentages, and anticorrelation of planktonic/benthonic foraminifer versus quartz/rock fragment contents.

F in an X-ray radiograph is displayed in Fig.9a.

Lithofacies succession, carbonate dissolution and early diagenetic textures

A characteristic facies succession occurs in the eastern cores along the investigated transect (e.g., core 23055-3, Fig.5; core 23065-3, Fig.6; core 23062-1, Figs.7 and 12). The most important discrepancy is a westward decrease in the numbers and thicknesses of dark lithofacies. Core 23059-1 (Fig.8) at the western end of the transect contains only a single dark layer a few centimetres above the base of the core. Dark facies were almost exclusively deposited during glacial stages (Figs.5–8). Stage 6 sediments contain the highest numbers and the entire thickness of dark lithologies. The facies succession commonly observed at the transition from a glacial to a well-developed interglacial stage, e.g., above and below the transition of isotope stages 10/9, 6/5 and 4/3, is as follows: Glacial lithofacies C is overlain by late glacial–early deglacial facies F and the interglacial facies B and A (Fig. 12). At the base of facies F, a sudden and major increase in input of ice-rafted debris is indicated by high percentages of quartz and rock fragments (Figs.5–7). Facies F is almost barren of planktonic and benthic foraminifers (Figs.5–7). Large dropstones and several centimetre-sized soft mud clasts, which are interpreted as mud dropstones, occur frequently (Fig.9). At the same level, a sudden increase in dissolution is detected by SEM indices (Fig.10). A pronounced change in the

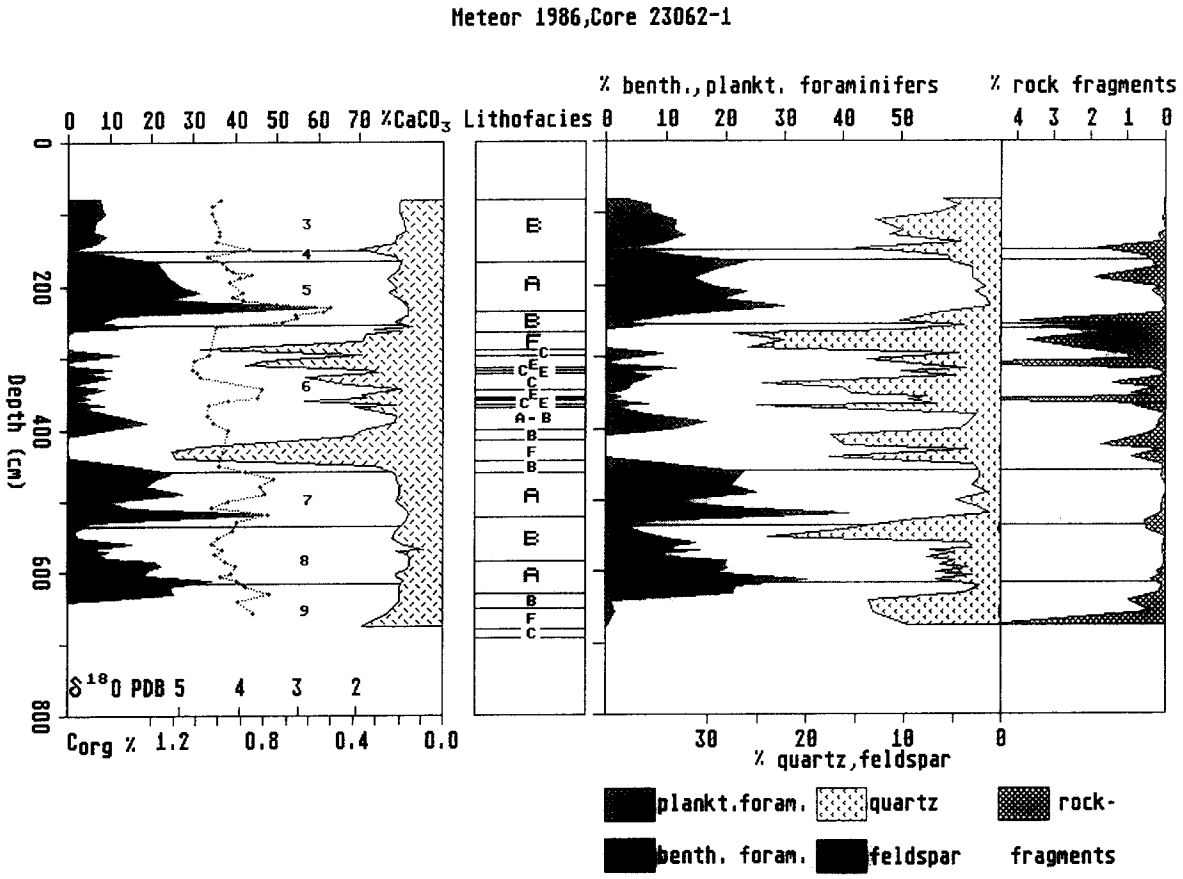

Fig.7. Basic sedimentology and oxygen isotope stratigraphy of core 23062-1. Note strong anticorrelation of bulk carbonate versus organic carbon weight percentages, and anticorrelation of planktonic/benthonic foraminifer versus quartz/rock fragment contents.

redox potential of the sediment towards anoxic conditions is demonstrated by a high percentage of sulphur (Fig.11; Kassens, Unpubl.) and iron (Fig.11).

A number of features in the topmost section of facies F, such as the change in colour to dark olive grey and thin iron laminations truncating sedimentary structures (mud clasts, Fig.9), indicate an early diagenetic overprinting of sediment similar to the basal lithology of facies F. These diagenetic features are truncated by younger burrows showing infillings of brownish sediments of the overlying facies B. Sediments of facies B are characterized by an upcore decrease in contents of quartz and rock fragments and large lithic dropstones (Figs.5–7). This decrease in terrigenous components coincides with an increase in the contents of the planktonic and benthic foraminifers (Figs.5–7), and a tendency towards better carbonate preservation (Fig.10). Sediments of facies B may include in their basal parts several up to 3 cm thick layers of facies E. These layers contain dropstones and mud clasts (Fig.9). Lithofacies A, on top of the entire succession (Figs.5–7), contains the highest contents of planktonic and benthic foraminifers and the lowest contents of quartz and rock fragments. Facies successions C, F, B and A are not only observed at the transition from glacial to interglacial stages, but are also found in lower stage 6 in cores 23055-3, 23065-3 and 23062-1 (Figs.5–7). Furthermore, additional dark layers of facies D and E are developed within some glacial stages, especially in stage 6 (Figs.5–7). Facies D and E are often intercalated within facies C.

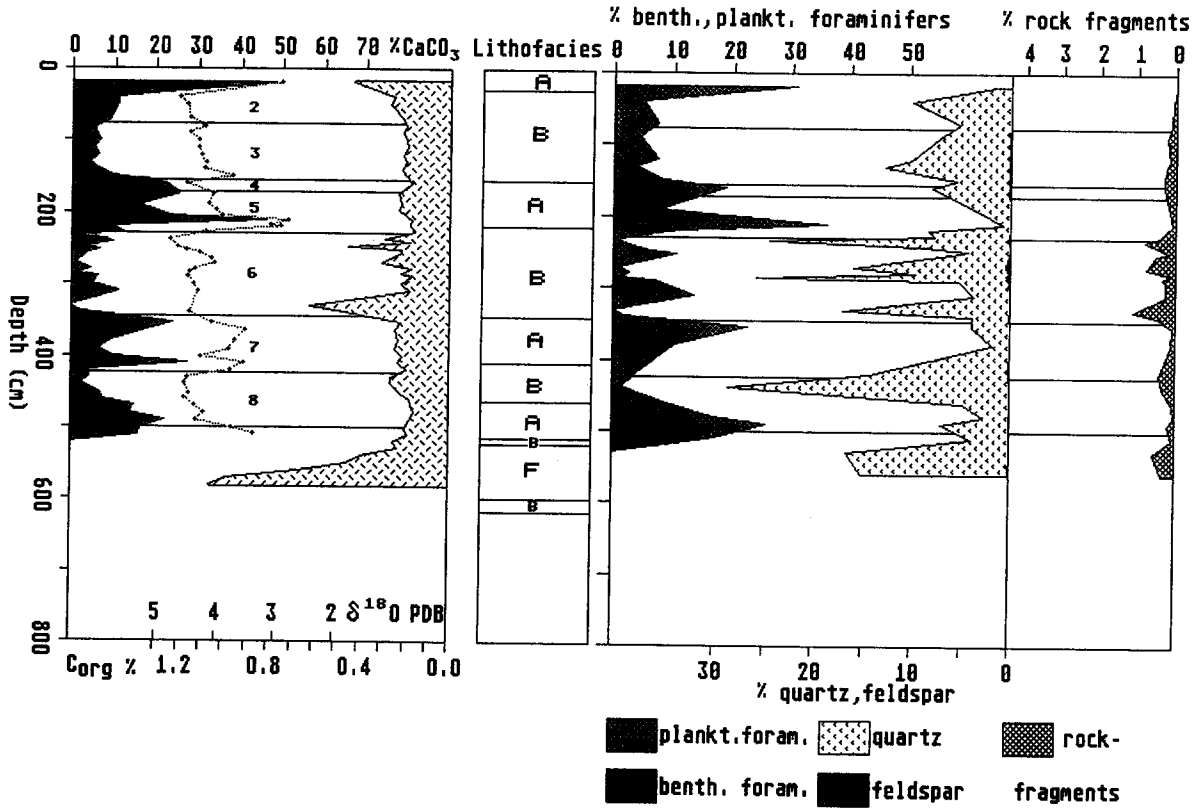

Fig.8. Basic sedimentology and oxygen isotope stratigraphy of core 23059-1. Note strong anticorrelation of bulk carbonate versus organic carbon weight percentages, and anticorrelation of planktonic/benthonic foraminifer versus quartz/rock fragment contents.

The alternation of dark and light lithofacies is strongly reflected by high-amplitude fluctuations in carbonate and organic carbon content, a feature which is best developed in stage 6. Low carbonate values, and in many instances, carbonate-free sections, coincide with high organic carbon values (above 0.5%, maximum 1.3%; Figs.5–7), and peaks in the SEM dissolution records (Fig.10). This pattern occurs almost exclusively in the dark lithofacies. Rock-eval analysis of organic carbon in these layers reveals kerogen type III, indicating as dominant sources terrigenous plants or reworked fossil organic carbon which is diagenetically altered (Henrich and Leythäuser, Unpubl.).

Regional and temporal distribution of lithofacies along the transect Vøring Plateau–Jan Mayen

The stratigraphic framework of the proposed lithofacies correlation is well defined by oxygen isotope stratigraphy (Fig.4). Stage boundaries established in the oxygen isotope records (Fig.3) are indicated by arrows reflecting the position of the respective stage boundaries in the core. Stage boundaries 4/3, 6/5 and 10/9 fall into almost carbonate-free sections of the cores. Some dark diamictons of facies F, e.g., those below the transitions 6/5 and 10/9 and within lowermost stage 6 can be traced from

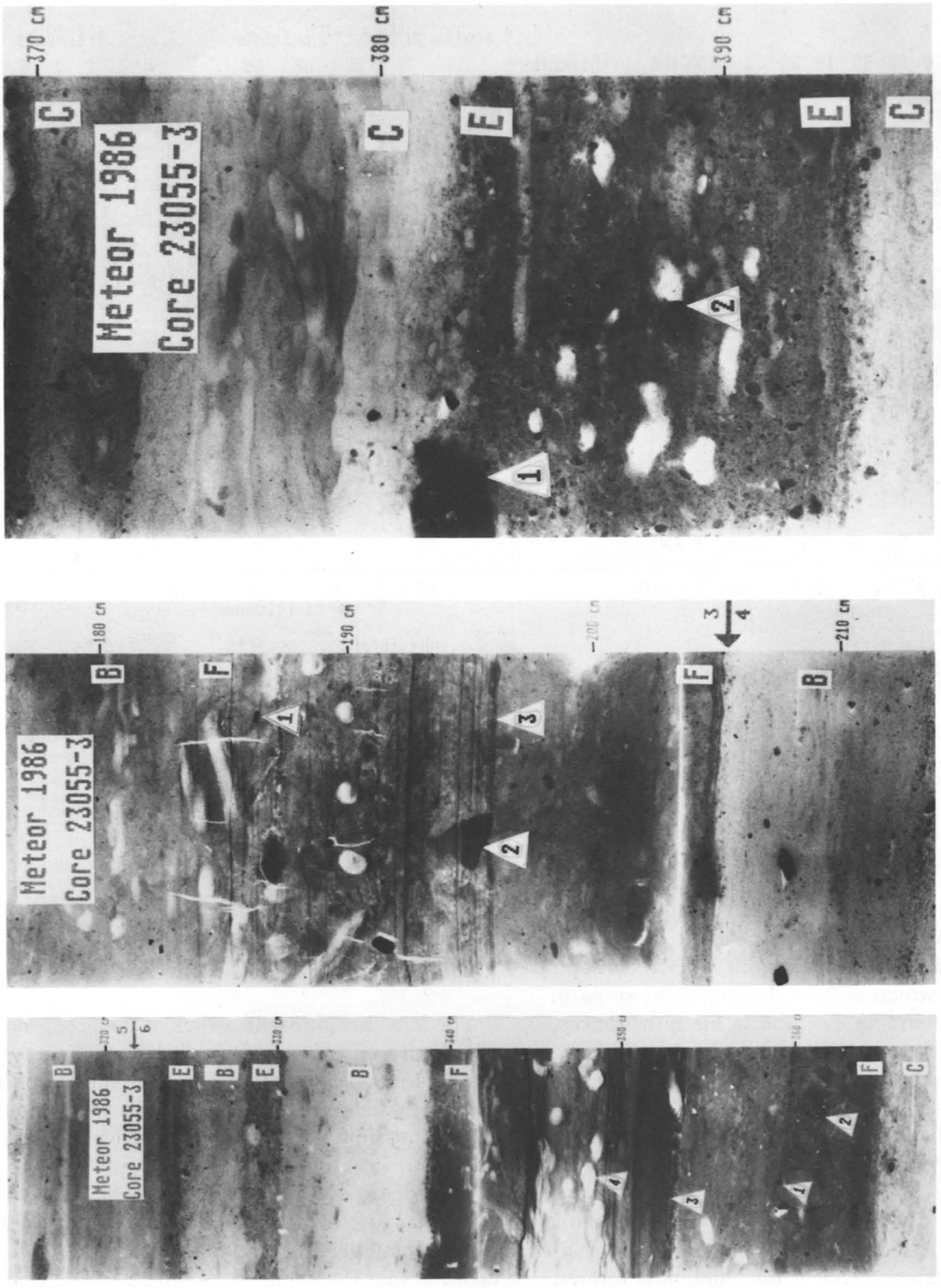

Fig.9.a. X-ray radiograph of lithofacies type F (complex diamicton). Note enrichment of coarse lithic *(1)* and mud dropstones *(2)* early diagenetic iron lamination *(3)* and younger oxic burrow fillings *(4)*. b. X-ray radiograph of lithofacies type E (dark olive grey diamicton). Note enrichment of coarse lithic *(1)* and mud dropstones *(2)*.

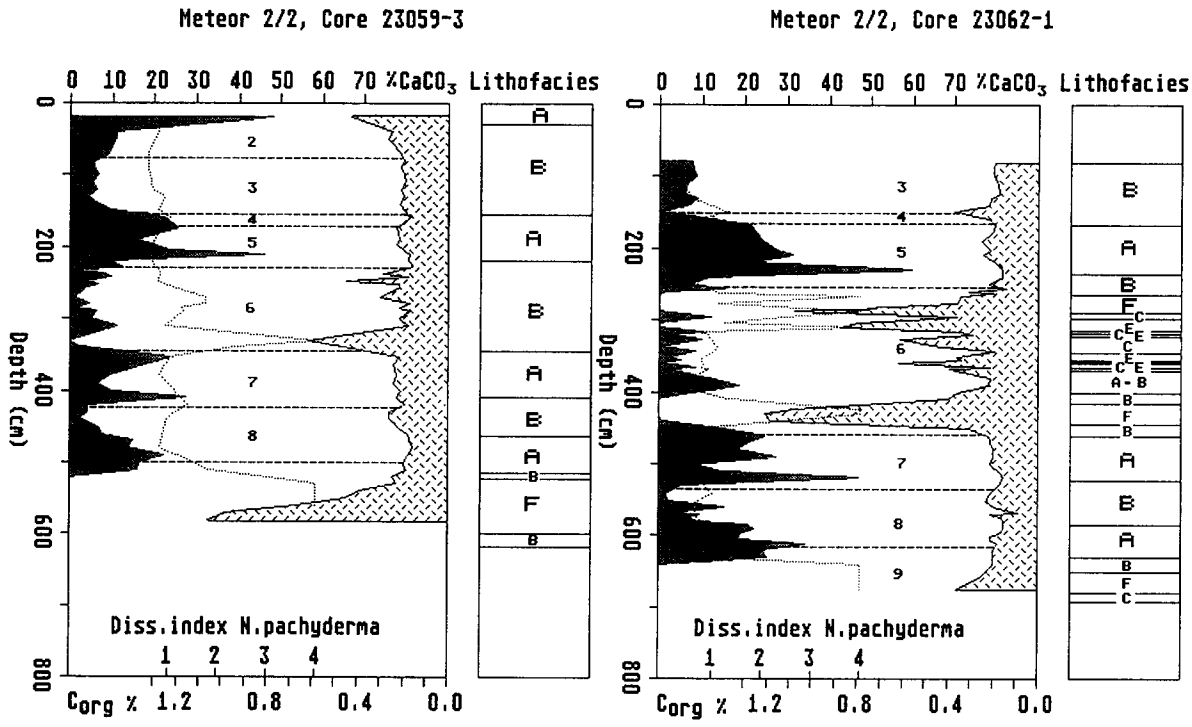

Fig.10. Dissolution records of cores 23059-3 and 23062-1. Note contemporaneous dissolution peaks in stage 6 that occur in dark lithofacies F and E in core 23062 and in brownish lithofacies B in core 23059.

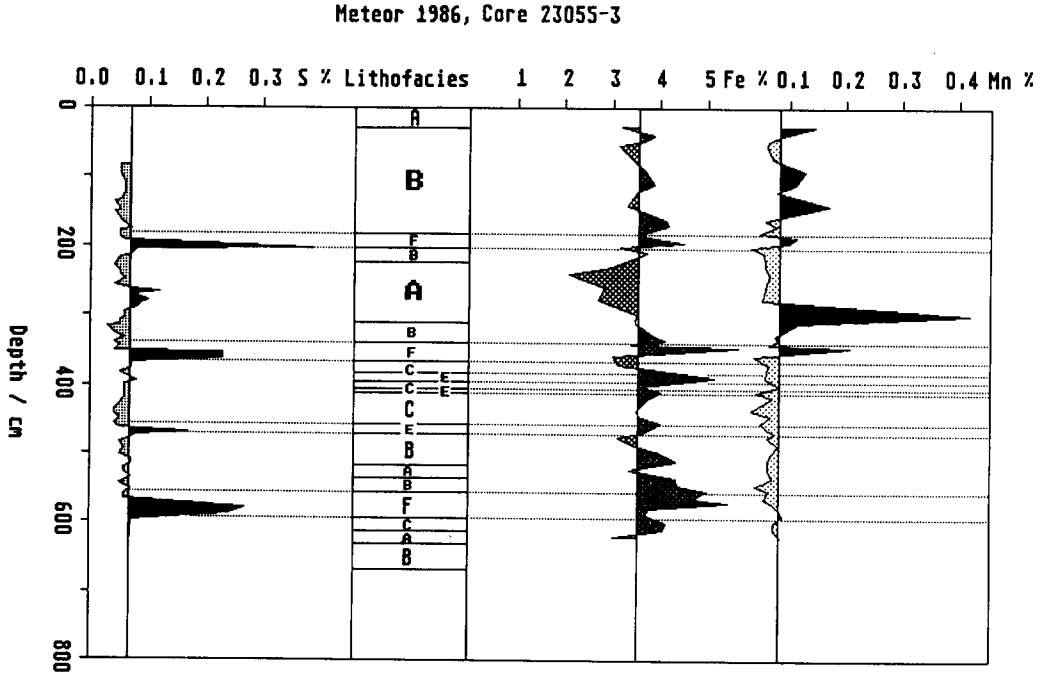

Fig.11. Iron, manganese and sulphur contents in core 23055-3. Note concentrations of iron and sulphur in the dark lithofacies F and E.

the Vøring Plateau far offshore to the west. In the west, such horizons (at transition 6/5 and in the lowermost stage 6) grade into a sediment layer of lithofacies type B (a brownish sandy mud with scattered dropstones) which is extremely enriched in coarse lithic dropstones. Only the dark diamicton horizon below the stage 10/9 transition occurs in all investigated cores. The

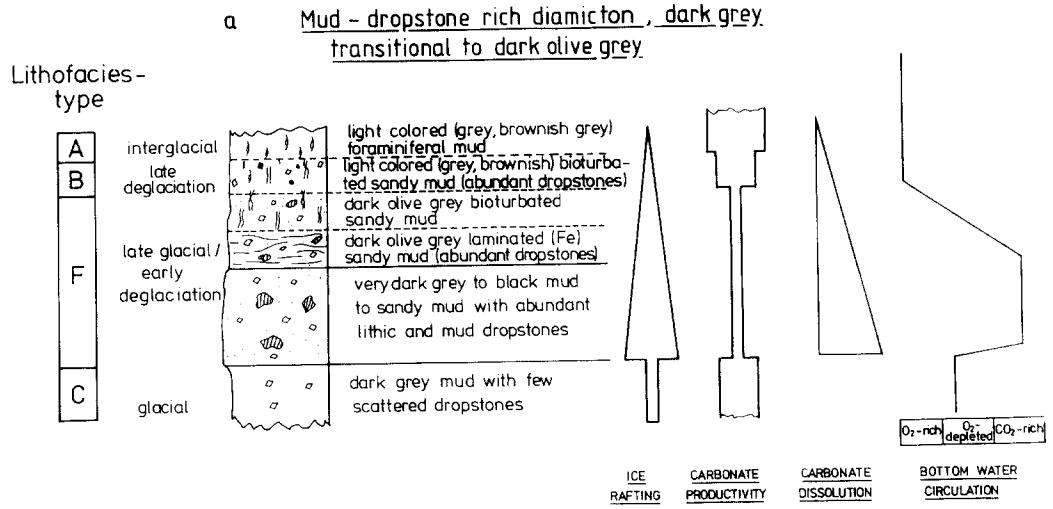

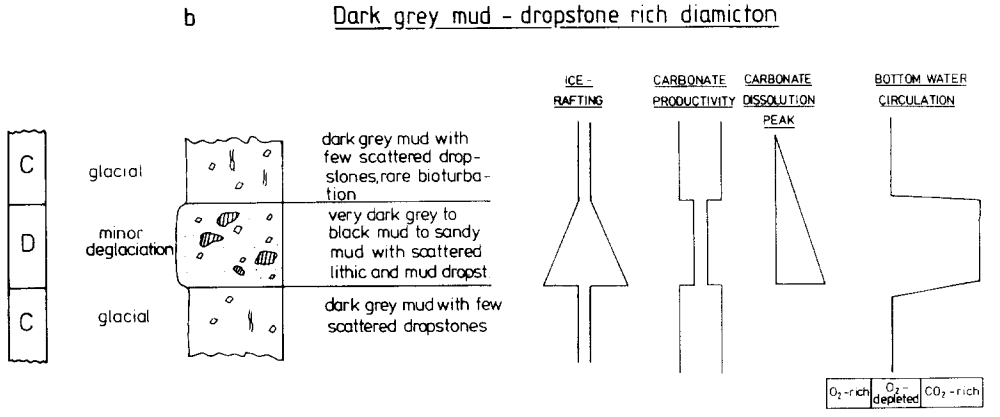

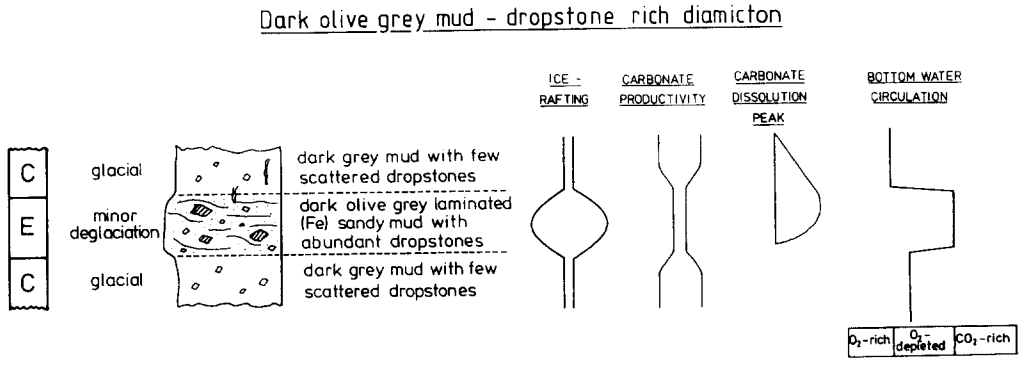

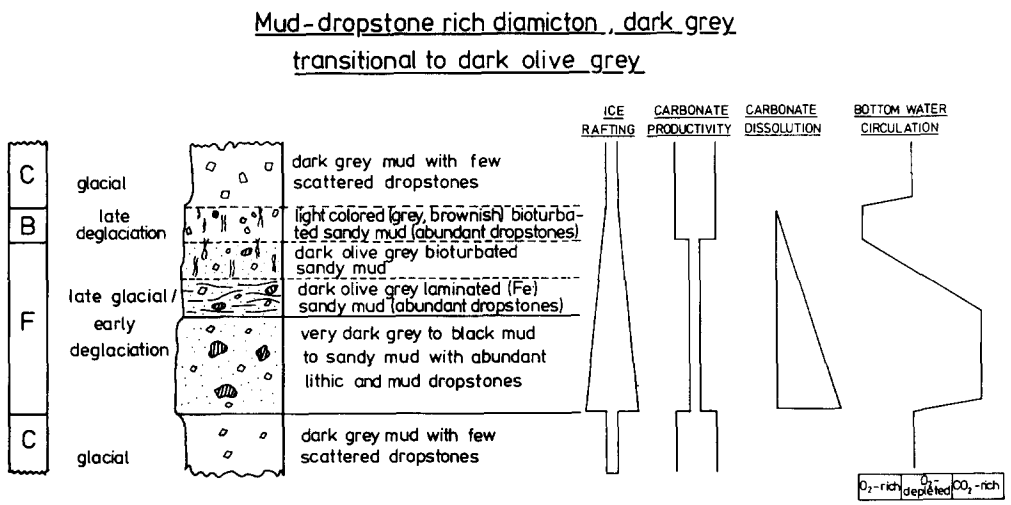

Fig.12. Compilation of basic lithofacies successions deposited during late glacial to interglacial periods (a) and during periods of maximum glacial advance and disintegration of the marine-based parts of the continental ice sheets (b). Environmental changes in surface and bottom water properties are indicated on a semiquantitative scale.

diamicton at the stage 4/3 transition is found only in the easternmost cores close to the Vøring Plateau (23055-3, 23068-1 and 23065-3) and grades westward into a dropstone-rich layer of lithofacies type B (cores 23062-1 and 23059-3).

Additional dark diamictons of facies D and E are intercalated within stage 6. In the easternmost cores (23055-3 and 23068-3), four thick layers are developed within stage 6. Westward, the number of thick layers de-

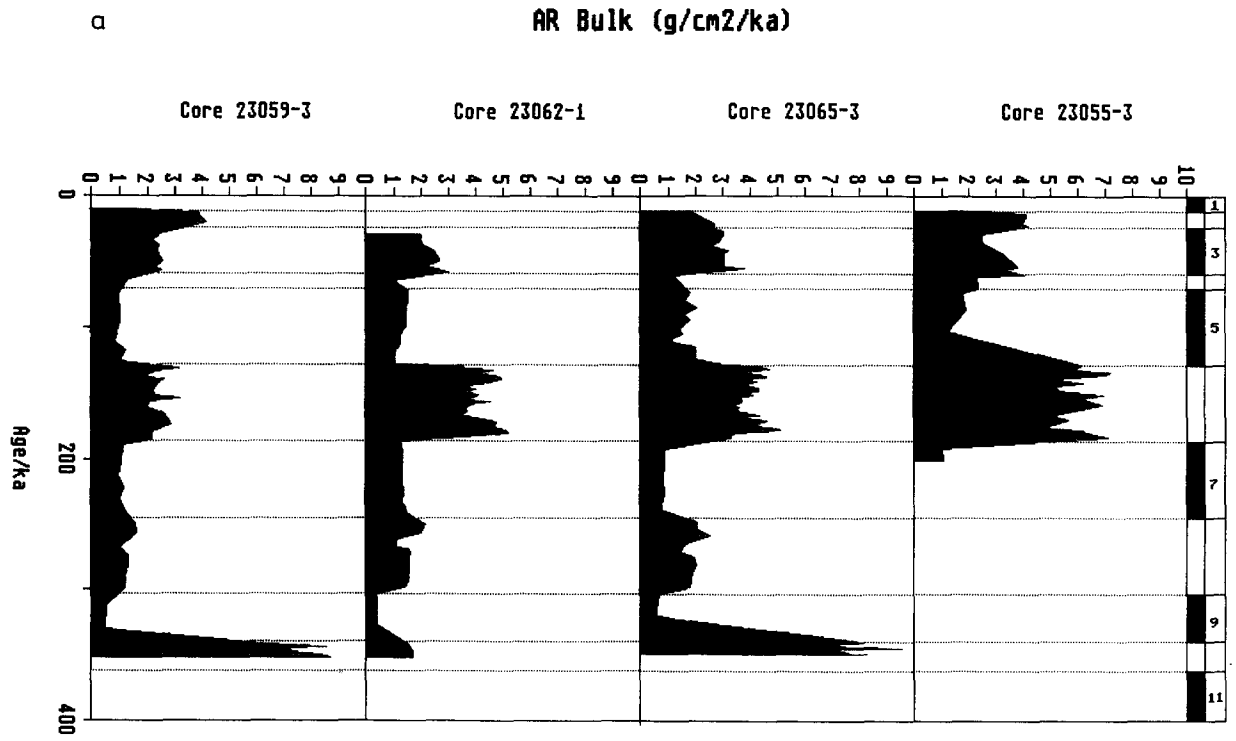

Fig.13. a. (*See caption, p.306.*)

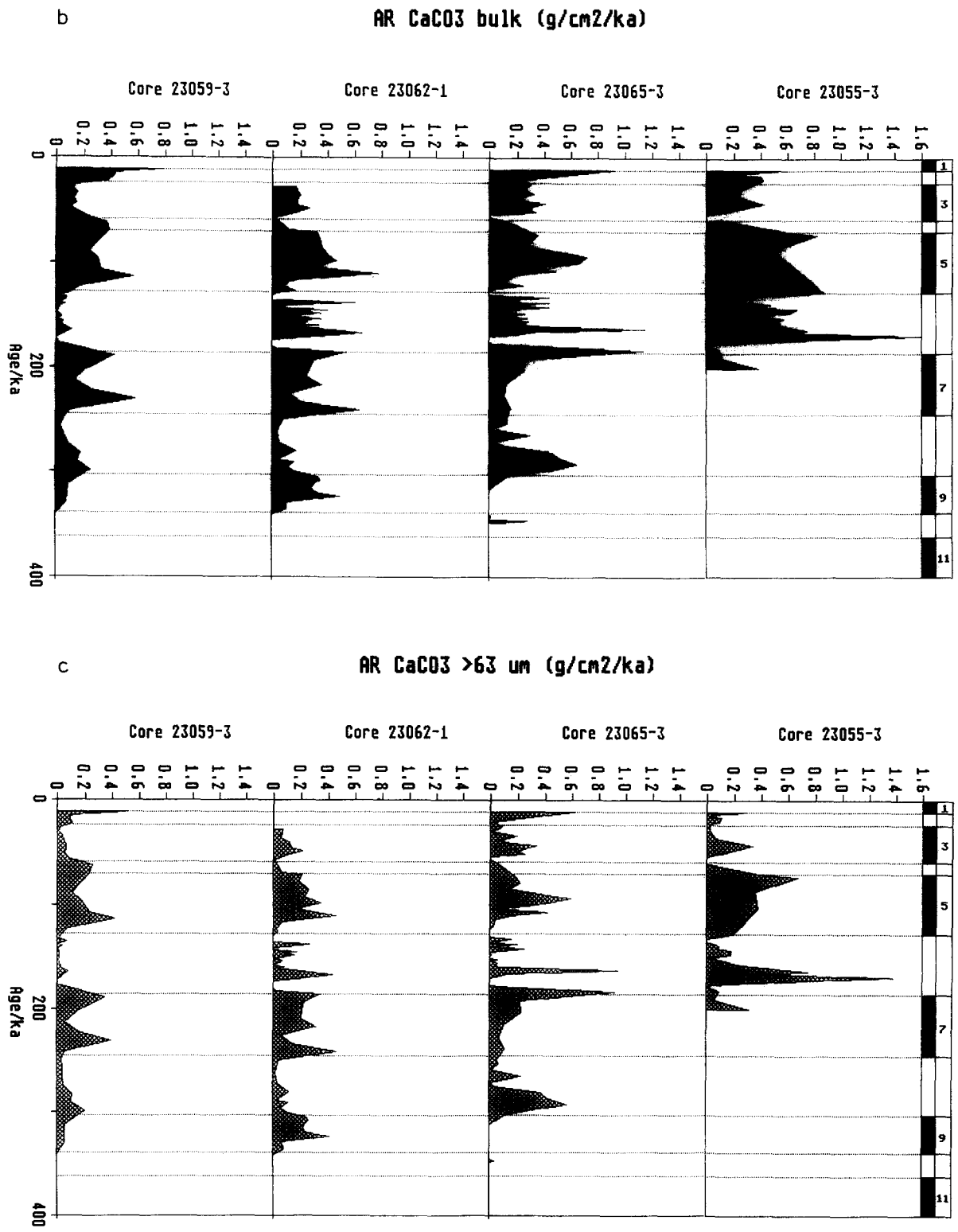

Fig.13. b and c. (*See caption, p.306.*)

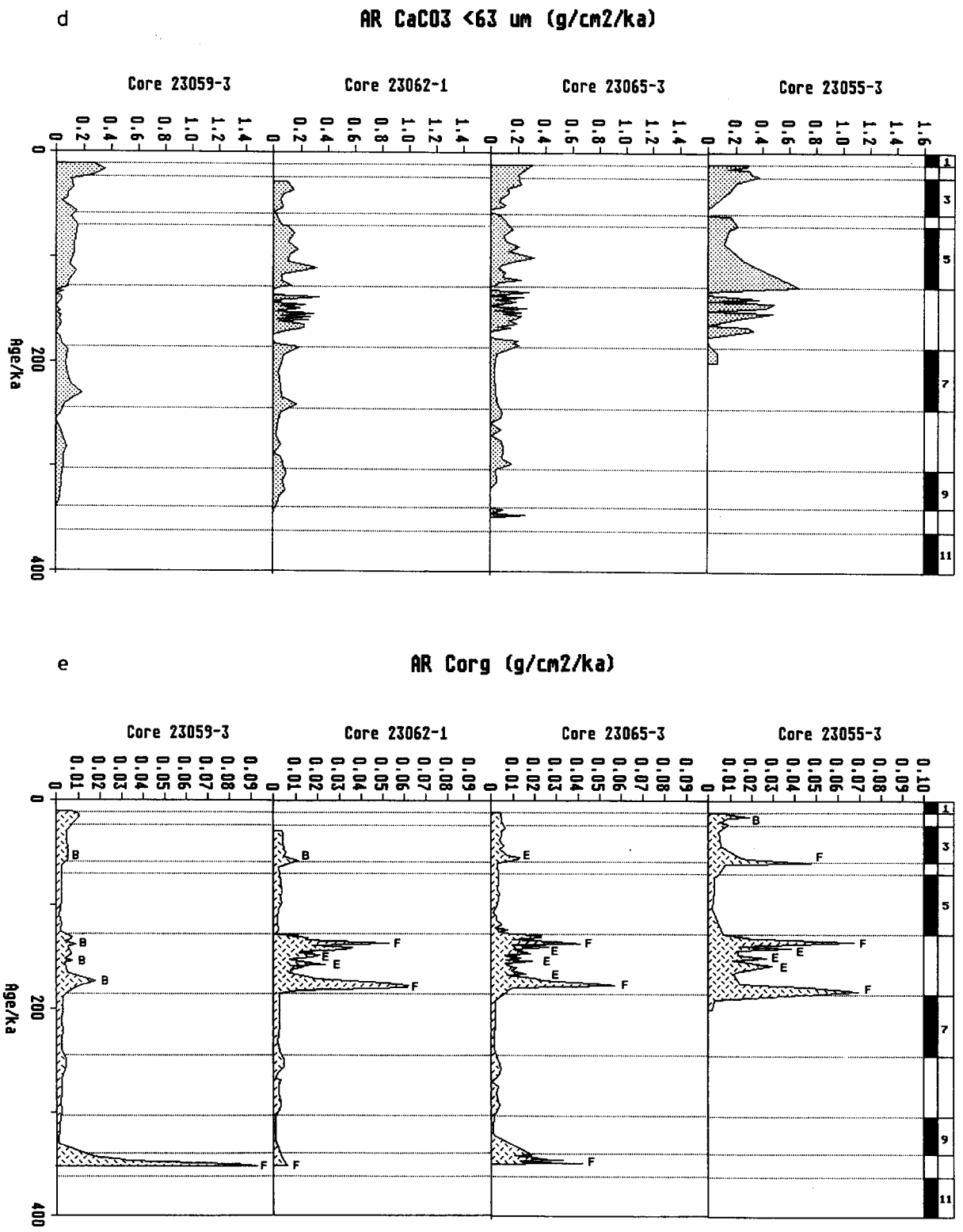

Fig.13. d and e. (*See caption, p.306.*)

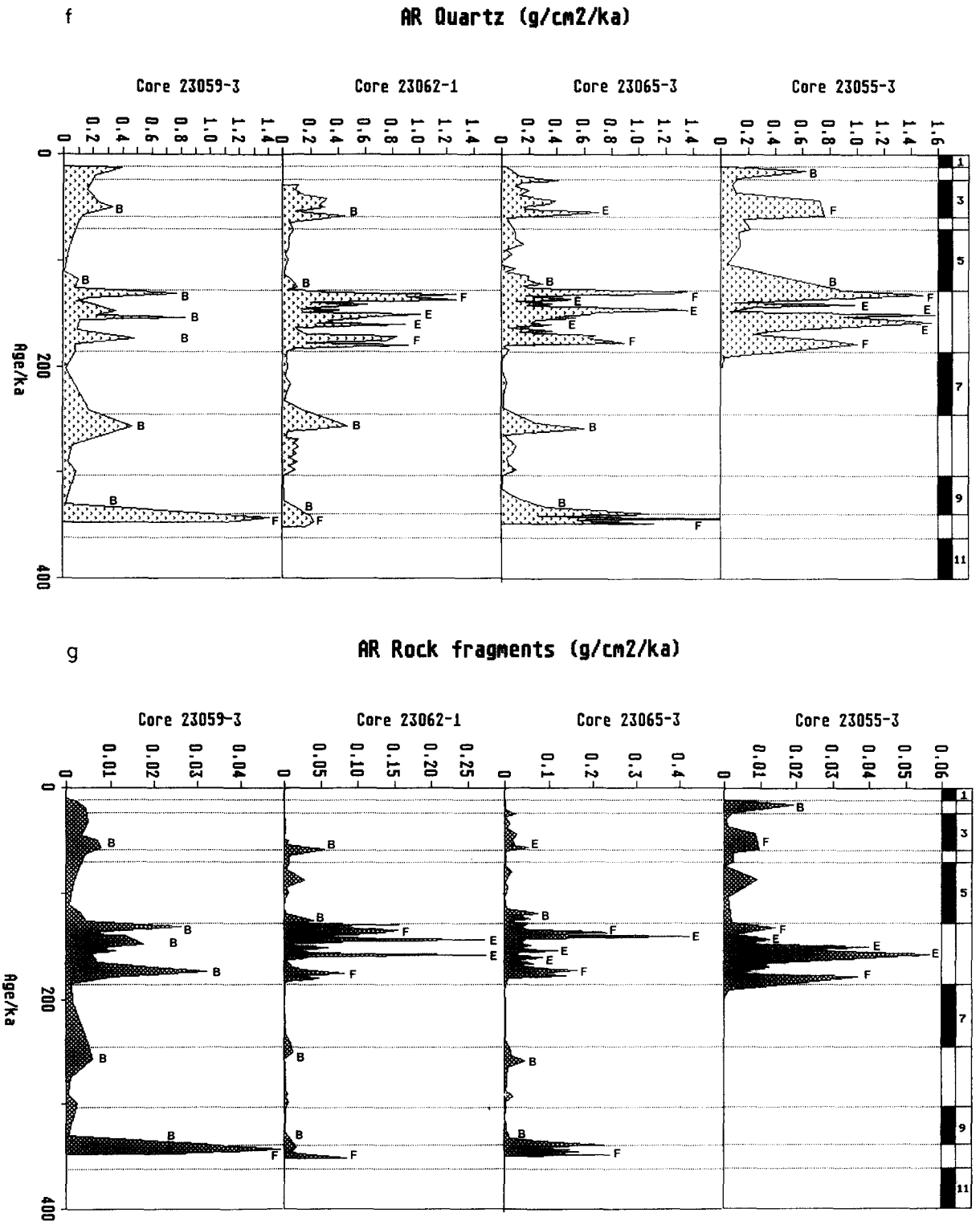

Fig.13. Fluxes of bulk sediment (a), bulk carbonate (b), coarse fraction carbonate (c), fine fraction carbonate (d), organic carbon (e), quartz (f) and rock fragments (g) along the investigated core transect.

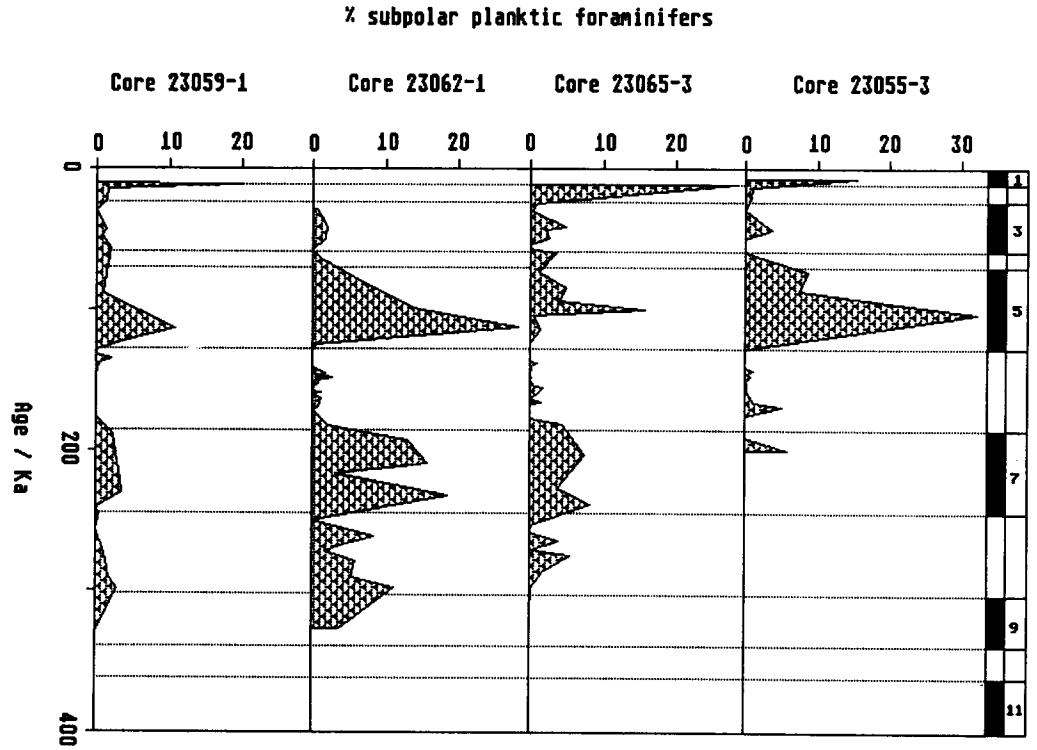

Fig.14. Weight-balanced percentages of subpolar planktonic foraminifers in cores 23059-1, 23062-1, 23065-3 and 23055-3 plotted against age.

creases progressively: three in core 23065-3, and two in core 23062-1, while none occur in the westernmost core, 23059-3 (see Fig.4).

Increased ice-rafted debris supply is also observed during the last termination, but has not formed a specific dark lithofacies type in all investigated cores. Instead, elevated concentrations of ice-rafted debris and some brownish and olive grey diagenetic iron laminations are found in one or two horizons of lithofacies type B.

Interglacial sediments of lithofacies type A, e.g., brownish foraminiferal muds and foram–nanno oozes, were deposited during stage 1, and parts of stages 3, 5, 7 and 9 in all investigated cores.

In summary, the regional distribution of dark lithofacies of types D, E and F shows a general decrease in frequency and thicknesses from the Vøring Plateau towards Jan Mayen. Individual layers can be traced westward where first a transition into oxic sandy muds with elevated dropstone concentrations is recognized, and finally a transition occurs into sediments with only occasional input of ice-rafted debris.

Long-term record of ice rafting, carbonate shell production and carbonate dissolution

Linear sedimentation rates (LSR), based on absolute age determination at the isotopic transitions, range between 0.4 and 6.3 cm/ka along the investigated palaeo-oceanographic transect during the last 350 ka (Table 3). Glacial stages generally have higher LSR values than interglacial stages. In the calculations of LSR (Table 3), carbonate-free sections with dark lithologies, which are developed a few centimetres below the isotopic terminations, have been included within the glacial sediment packages.

The general westward decrease in dark diamictons is reflected in the LSR and the bulk

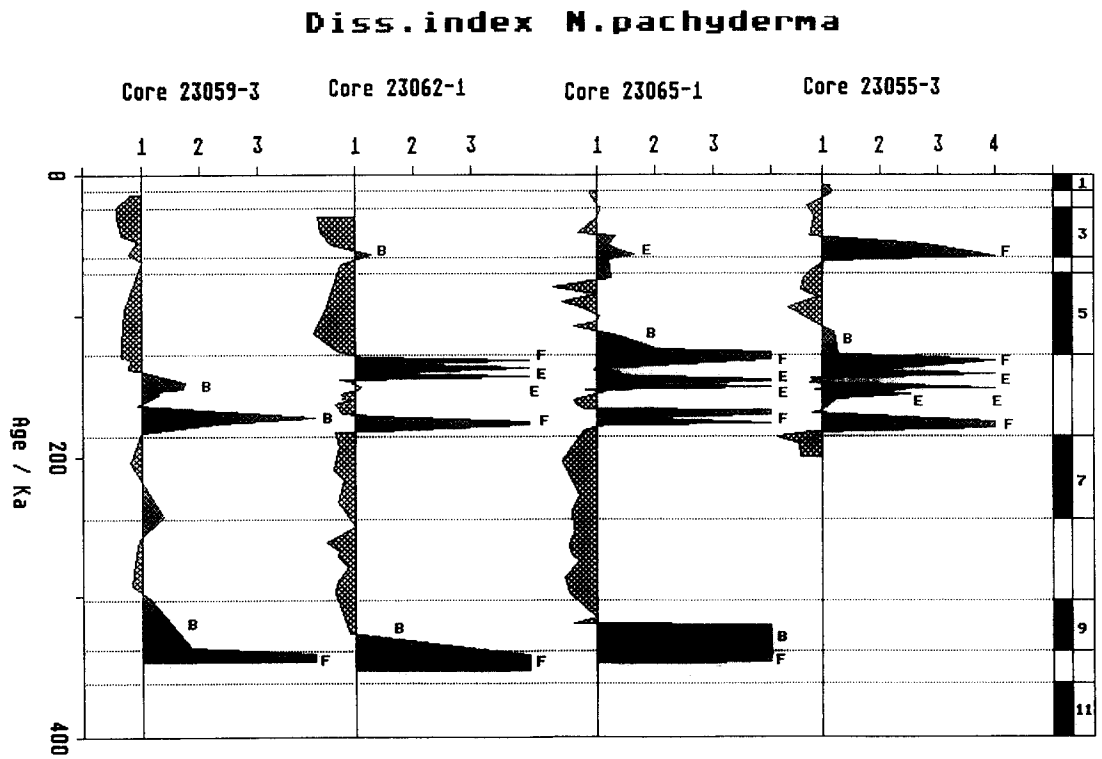

Fig.15. Dissolution records of cores 23055-3, 23065-1, 23062-1 and 23059-3 plotted against age. Note contemporaneous dissolution peaks that occur in sediments of facies F and E in the eastern cores and facies B in core 23059-3.

sediment fluxes (bulk accumulation rates, Fig.13a). The highest LSR and bulk sediment fluxes were established during stages 2, 3 and 6. The total sediment flux during stage 6 attains values of 6–7 g/cm^2/ka over the Vøring Plateau (core 23055-3). It decreases to 4–5 g/cm^2/ka in the middle part of the transect (cores 23065-3 and 23062-1), and in the westernmost core (23059-1) fluxes are at a very low level of 2–3 g/cm^2/ka. Peak inputs of total sediment correlate well with dark lithofacies in the eastern cores (Fig.13a). The corresponding brownish, dropstone-rich lithologies in the western cores also show elevated bulk accumulation rates.

In contrast, the low to intermediate interglacial LSR (stages 1, 5, 7 and 9) are quite stable along the transect. During stages 5 and 7 bulk accumulation rates are just above 1 g/cm^2/ka in all cores. Stage 9 has very low linear sedimentation (0.8–0.4 cm/ka) and bulk accumulation (0.3–0.5 g/cm^2/ka) rates. These generally low levels in interglacial LSR and bulk sediment fluxes indicate a low supply of terrigenous matter from the Norwegian continent.

Total carbonate fluxes are generally highest during interglacial stages, averaging between 0.2 and 0.9 g/cm^2/ka, which is 30–60% of the bulk sediment flux (Figs.13a and b). Typical glacial carbonate fluxes (0.2–0.4 g/cm^2/ka) attain only 5–20% of the bulk flux (Figs.13a and b). The highest proportions of carbonate relative to bulk sediment fluxes are observed during stage 5, especially during stage 5e (40–60%). This increase probably indicates an increase in the strength and warmth of the Norwegian Current. The generally low to intermediate carbonate fluxes during stages 7 and 9 reflect weak interglacial circulation. The high carbonate accumulation rate during early stage 8 in core 23065-3 (0.6–0.8 g/cm^2/ka) may indicate the presence of warm Atlantic Surface Water in the eastern sector of the transect.

Percentages of subpolar planktonic foraminifers (Fig.14, values are balanced to bulk

sediment weight) indicate similar variations in interglacial circulation patterns. Highest percentages of subpolar planktonic foraminifers (15–30%) are recorded during stages 1 and 5e. Much lower values (5–10%) were found in stage 7 deposits. In addition, minor amounts of subpolar planktonic foraminifers were identified during events 3.3, 6.5 and the lower part of stage 8 (Fig.14).

During stage 6, episodic high carbonate accumulation rates (0.6–1.6 g/cm^2/ka) were determined from LSR calculations. However, stage 6 sediments include the highest frequency and the entire thickness of dark lithofacies. Hence, the high carbonate accumulation rate may be an artifact of the calculation method. The basic assumption of an LSR for all stage 6 deposits may be invalid. Assuming differential sedimentation rates with much higher values for the dark lithofacies and lower values for the carbonate-bearing deposits would possibly result in more realistic carbonate flux calculations. Since a detailed stratigraphic resolution within stage 6 may be hampered by regional salinity or temperature effects (Ramm, 1988; this study), this problem must be resolved in future investigations.

On a regional scale, highest carbonate fluxes are observed over the Vøring Plateau, with a minor decrease towards the central section of the transect and a more pronounced decrease towards the westernmost core (Fig.13b). A second major trend is the general dominance of coarse-fraction carbonate along the investigated transect. During some glacial periods (e.g., parts of stages 2, 4 and 6) fine-fraction carbonate dominates. Today, high calcareous nannoplankton production of fine-fraction carbonate is restricted to the region influenced by the Norwegian Current. Therefore, high proportions of fine-fraction carbonate in the glacial fluxes may be due to deposition of eroded fossil carbonates, e.g., Cretaceous to Tertiary chalks.

Fluxes of ice-rafted quartz and rock fragments (Figs.13f and g) and total organic carbon (Fig.13d) are strongly episodic. Rapid increases in the flux of total organic carbon and ice-rafted debris occur during deposition of dark lithofacies within stage 6, and below the stage of 10/9, 6/5 and 4/3 transitions. The westward decrease in sedimentation of mature organic matter (kerogen type III, see above) suggests supply from eroded terrigenous organic matter-rich sediments outcropping on the shelves. Carbonate dissolution (Fig.15) is confined to dark lithofacies horizons as shown by increased organic carbon fluxes and coarse-grained quartz and rock fragment accumulation rates, and the SEM dissolution records (Figs.13e–g and Fig.15).

In summary, the spatial and temporal pattern of sediment fluxes can be attributed to variations in the two important sediment sources in the Norwegian Sea: carbonate productivity in surface waters and input of ice-rafted and resuspended debris derived from Scandinavia and Greenland. In general, when carbonate productivity is highest, e.g., during warmest interglacials with a high sea level, the supply of sediment is mainly limited to "pelagic rain" from the Norwegian Current. Low to intermediate fluxes occur at this time, because terrigenous material is mostly stored on the continental shelf. Maximum inputs of ice-rafted and resuspended debris occur in late glacial–early deglacial times and episodically within glacial periods when sea level is low or rising and terrigenous material is transported into the deep sea (see Thiede et al., 1986).

Palaeo–oceanographic model and early diagenesis of glacial and late glacial–early deglacial sediments

All sedimentological and early diagenetic observations have been integrated in a conceptual model describing stepwise changes in bottom- and surface-water circulation during the transition from glacial conditions to full interglacial environments. The proposed palaeo–oceanographic settings are illustrated schematically in block diagrams (Fig.16).

The situation recorded in lithofacies type C (Fig.16a) represents a period of strong glaciation indicated in the sediments by the low

content of ice-rafted debris (Figs.5–8) and reduced carbonate productivity (Figs.13b–d). During severe glaciation the Scandinavian ice sheet extended towards the Norwegian shelf edge. King et al. (1987) present maps based on seismic interpretations that show till tongue distribution patterns on the mid-Norwegian shelf. Till tongues were found close to and below the shelf edge at water depths of greater than 400–600 m. Large amounts of shelf sediments may have been incorporated into the basal parts of the glacier ice during advance. Offshore sea-ice cover most likely fluctuated between complete cover during winter, and

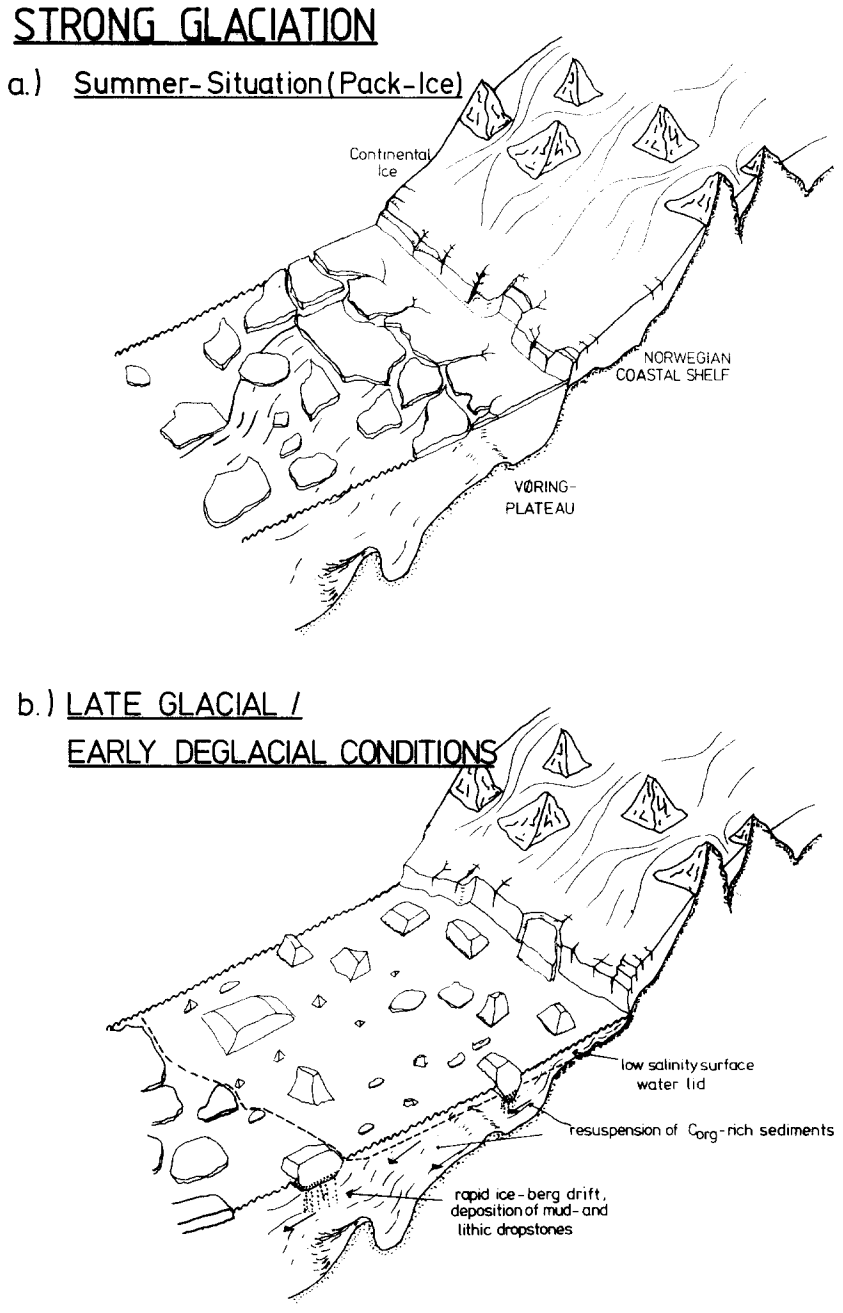

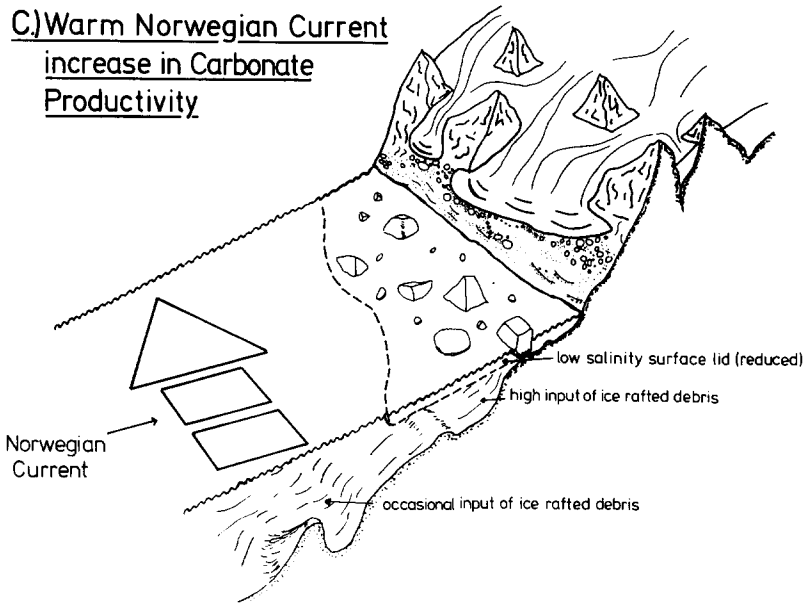

Fig.16. Conceptual palaeoenvironmental model. a. Strong glaciation reflecting advance of continental ice on the Norwegian coastal shelf associated with offshore packice drift. b. Late glacial–early deglacial strong iceberg drift induced by surges of the marine-based parts of the continental ice; surface water connection with the North Atlantic may be partially blocked off by large iceberg barriers. c. Intrusion of the Norwegian Current with retreat of iceberg drift progressively closer to the coastal regions and offshore increase in carbonate productivity.

summer packice interspersed with a few drifting icebergs.

During the maximum advance of continental ice onto the Norwegian shelf, large-scale calving of icebergs, possibly supplied by surges along the ice front, would contribute huge numbers of icebergs into the southern sector of the Norwegian Sea (Fig.16b). Iceberg drift in this region might partially block off surface-water connections with the North Atlantic by piling up large ice barriers along the Iceland–Faroe–Shetland Ridge (Wohlfeil, 1982, 1983). Surface-water environments would then be affected by fast-dropping ice-rafting (see Figs.5–9 and 13e–g) and reduced surface-water salinities, such as in the modern Arctic (Swift, 1986). Deep-water renewal and circulation in the eastern Norwegian–Greenland Sea would be depressed, resulting in oxygen-depleted conditions. Calved icebergs would distribute incorporated sediments including frozen mud dropstones. Rapid accumulation of ice-rafted debris would be accompanied by resuspension of organic matter possibly derived from reworked, organic carbon-rich sediments. Oxidation of marine organic matter at the seafloor and decreased renewal of bottom water would cause increased dissolution of the already reduced pelagic rain of carbonate tests from the surface waters. In addition, rapid burial of reworked terrigenous organic matter would contribute a relatively stable organic phase that causes the elevated organic carbon contents of the sediments.

With the beginning of deglaciation, sea level would rise and a progressive northward intrusion of the Norwegian Current would occur (Figs.16b and c). The rapid rise of sea level most probably caused sudden disintegration of the marine-based parts of the continental ice sheet. Glacier surging, with large-scale calving of icebergs into the sea, is the scenario envisaged along the Norwegian coast. Surface waters would be affected by sediment-laden meltwater suspensions introduced from the base of large tidewater-glacier fronts on the

shelf (Molnia, 1983; Powell, 1983; Pfirman and Solheim, this issue). Meltwater from the combined effects of melting icebergs and glacial meltwater discharge would form a surface low-density layer reducing surface productivity and inhibiting vertical mixing.

In lithofacies types B and A, an increase in carbonate productivity in the Norwegian Current (Figs.13b–d) concomitant with a decrease in ice rafting is observed (Figs.13e–g and Fig.16c). Vertical mixing is reactivated and bottom waters return to less oxygen-depleted conditions across the entire basin. Rapid exchange of bottom water and increased production of Norwegian Sea Deep Water (NSDW) in the western and northern sectors of the Norwegian–Greenland Sea result in good carbonate preservation at the seafloor (Fig.14).

Depositional and early diagenetic features detected in the late glacial–early deglacial sediments are summarized in Fig.17. High carbonate corrosivity of bottom waters resulted from oxidation of marine organic matter at the seafloor and reduced exchange of bottom water. Resuspension of additional organic matter eroded from shelf sediments contributed significantly during sedimentation. Because of the predominant maturity of the organic carbon deposited in facies D–F, considerable amounts were not oxidized but buried with the sediment. Anoxic conditions were already achieved during incipient burial. Anoxic conditions within the sulphate reduction zone caused precipitation of monosulphides.

During later stages of early diagenesis (e.g., during the deposition of the oxic sediments of facies B and A on top of the anoxic sediments of facies D–F), secondary oxidation occurred by downward diffusion of oxic pore waters and upward diffusion of reduced iron and manganese. This secondary oxidation affected the topmost layers of facies D–F. Iron hydroxide or iron oxide crusts were precipitated causing incipient lithification of this layer. Manganese precipitated at a higher level within the oxic brownish layers as dark manganese oxide bands (see the iron and manganese profiles in core 23055-3, Fig.11). The very early formation of these layers is confirmed by burrows trun-

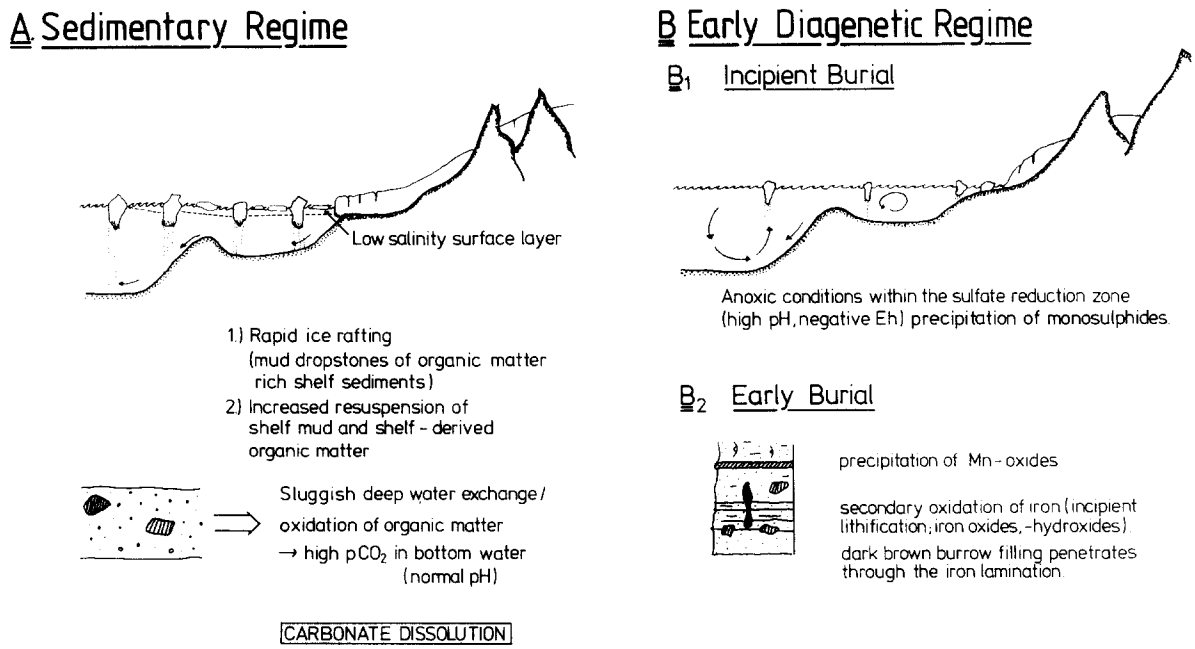

Fig.17. A and B. Model of early diagenetic processes in late glacial–early deglacial sediments.

cating the iron bands and filled with oxic sediments. Assuming a vertical penetration of the *Planolites* type of burrows similar to that in the modern Arctic environment (10–20 cm), using LSRs one may calculate the maximum time span between formation of the diagenetic iron lamination and the onset of the burrowing activity as being in the order of 1–3 ka.

The palaeo-oceanographic scenario outlined above is substantiated by the regional distribution of dark diamictons along the investigated transect (Fig.4 and previous sections). The greatest thicknesses and highest frequencies of the diamictons occur close to the continental margin, they decrease in number and thickness westward and grade far offshore into oxic sediments that again reflect a westward decrease in dropstone concentrations. Fluxes of ice-rafted debris and organic carbon (Figs. 13e–g) also have peak inputs close to the coast, gradually diminishing westward. In most instances, layers of facies F do not occur exactly at the transitions in the oxygen isotope records. At termination II they end 8 cm below in core 23062-1 (Fig.7), and 19 cm below in core 23055-3 (Fig.5), corresponding to an age of 130 ka (core 23062), and 132 ka (core 23055) based on LSRs. As already mentioned in the previous sections, facies B overlying facies F contains two layers of dark facies E, 2–3 cm in thickness. These layers appear close to termination II, providing evidence that the principal mechanisms, discussed above, were still operating during termination II. Nevertheless, there is a clear time lag of 2–3 ka between the major late glacial–early deglacial sediment input into the Norwegian Sea and the major warming recorded in the oxygen isotope records. This indicates that these large inputs of ice-rafted debris may record late glacial to very early deglacial periods when marine-based parts of the continental ice on the shelf surged, causing extensive ice rafting. With the progressive intrusion of the Norwegian Current and deglaciation, melting of the remaining ice cap over the Scandinavian continent resulted in meltwater discharge and iceberg release progressively closer to the coast. Meanwhile, carbonate production increased in surface waters further offshore.

Less complete late glacial–early deglacial sequences (i.e., intercalations of facies D, E or F in facies C; see Figs.4 and 12) were most commonly established during glacial stages when a weak intrusion of Atlantic water into the southeastern Norwegian Sea or a small sea-level rise caused surging along the front of the marine-based continental ice sheets. Also, huge icestreams on the shelves may have rapidly released icebergs. Warming may have occurred during these periods, but a normal interglacial Norwegian Current with its typically high carbonate productivity (Figs.13b–d) did not develop. Additionally, vertical mixing and, therefore, oxygenation of bottom waters during these "minor deglaciations" was less efficient, resulting in a reduced oxygen level in the bottom waters.

Discussion

Glacial–interglacial cycles primarily reflect the climatic response of the atmosphere–ocean system to cyclic fluctuations in the Earth's orbital parameters, e.g., Milankovitch cycles (Imbrie et al., 1984). Various feedback mechanisms influence the oceanographic response in glacials and interglacials, such as (1) the increase in albedo during the growth of the ice sheets, (2) rapid meltwater discharge during deglaciations to parts of the world's oceans (Olausson, 1985), (3) tropical rain forest growth (Shackleton, 1977), and (4) coral reef growth (Berger, 1982). In high latitudes, some of these feedback mechanisms result in complex interactions between the atmosphere and oceans. Ruddiman and Glover (1975) and Ruddiman and McIntyre (1981) have demonstrated that the last deglaciation in the high-latitude North Atlantic occurred in three steps: at 13 ka in the southeast sector, at 10 ka in the central and northern sector, and at 9–6 ka in the Labrador Sea.

Recent high-resolution studies of the last deglaciation period in the Norwegian Sea indicate a complex pattern of changes in

surface- and bottom-water circulation which were partly out of phase with the North Atlantic. Before 12 ka, ice rafting and low carbonate productivity dominated the surface-water environment (Jansen et al., 1983; Sejrup et al., 1984; Henrich, 1986), while reduced deep-water formation (Jansen and Erlenkeuser, 1985) and increased resuspension of organic matter resulted in increased carbonate dissolution (Henrich, 1986). At about 12 ka, the influx of Atlantic water is reflected by high diatom productivity and the first reappearance of coccoliths and radiolarians in the southern Norwegian Sea (Jansen and Bjørklund, 1985). Deep-water formation may have been reinitiated shortly after 12 ka, as carbonate dissolution gradually diminished during termination Ib (10–8 ka) (Henrich, 1986). Ice rafting still dominated the surface-water environment of the Voring Plateau during termination Ib (8 ka). Since then, a gradual elevation of carbonate productivity occurred (Henrich, 1986).

Even larger fluctuations in meltwater discharge and supply of ice-rafted debris into the Norwegian Sea have occurred throughout glacial–interglacial cycles of the past 350 ka. A westward decrease in contents of ice-rafted debris in Norwegian Sea glacial sediments was recognized by Holtedahl (1959). Kellogg (1976) detected two foraminifer-barren zones in various Norwegian Sea cores which coincide with the dark lithofacies occurrences at the stage 4/3 and 6/5 transitions in the studied cores. Kellogg (1976) proposed that rapid ice rafting might have contributed to the formation of the barren horizons. Flux calculations of ice-rafted debris supply into the North Atlantic and Norwegian–Greenland Sea by Ruddiman (1977) outlined major pathways and sources of ice rafting in the northern seas. Icestream patterns compiled by Ruddiman (1977) show a predominantly westward flow of continental ice on the Norwegian shelf.

Flux data from our study are based on high-resolution isotope stratigraphy, and thus provide additional quantitative information. Fluxes of ice-rafted debris appear to be strongly episodic. Individual peaks can be traced continuously westward where they decrease in magnitude. Another new finding is the correlation of peak input in ice-rafted debris with peak fluxes in terrigenous organic matter and carbonate dissolution. Broecker (1982) stressed the importance of input of resuspended terrigenous organic carbon to the oceanic carbon balance during glacial maxima. High terrigenous organic carbon concentrations in the dark lithofacies layers in the Norwegian Sea sediments provide evidence for Broecker's proposition. Winnowing and resuspension of terrigenous organic matter, possibly reworked from shallow-marine outcrops on the shelves during glacial advance of the continental ice sheets, and oxidation of marine organic matter, episodically resulted in highly corrosive deep waters in the Norwegian Sea.

A number of results from previous studies support the basic assumptions of the conceptual palaeo-oceanographic model proposed in the previous section. King et al. (1987) mapped till tongue occurrences along the edge of the mid-Norwegian shelf at water depths deeper than 400–600 m, providing evidence that during severe glaciation the shelf was entirely covered by several hundred metre-thick continental ice sheets. Hald and Vorren (1987) presented combined sedimentological and isotopic evidence for a strong influence of meltwater discharge along coastal regions off northern Norway during termination I. Lowered salinities caused by high meltwater discharge possibly resulted in episodic stratification of water masses (Berger and Vincent, 1986) and affected deep-water formation in the Norwegian–Greenland Sea.

The mode and the possible cessation of deep-water formation in the Norwegian–Greenland Sea during glacial and deglacial periods have been the subject of numerous studies (see a review by Corliss et al., 1986). Streeter et al. (1982) concluded from benthic foraminifer evidence that the Norwegian–Greenland Sea was not a source of deep-water outflow during isotope stages 5d to 2. In contrast, Boyle and Keigwin (1982) proposed a continuous flow of

NADW during glacials, but stated that the flow rate was only about half of the present magnitude. Hence, either the Norwegian–Greenland Sea may not have been a sink for dense surface waters (Kellogg, 1980; Streeter et al., 1982), or deep water may have formed by mechanisms other than those prevailing today (Mix and Fairbanks, 1985; Jansen et al., 1988). Labeyrie and Duplessy (1985) assume a strongly divergent cyclonic cell in the 18 ka North Atlantic based on a comparison of sea-surface temperature distributions and $\delta^{13}C$ analysis of *N. pachyderma*. On the northern flank of this gyre, centred at approximately 55°N, 15°W, deep-water formation would be possible, analogous to the present situation in the Weddell Sea. Deep-water formation within the Norwegian–Greenland Sea could also occur as follows: Surface cooling and evaporation over wide areas of the Norwegian–Greenland Sea may have been induced by strong katabatic winds blowing from the large continental ice sheets or large-scale seasonal sea-ice formation during winter. Dense surface waters formed in this way could convectively overturn and contribute to deep water. A complete shut-off of deep-water formation during glacial periods seems improbable, because dissolution records (Fig.15) indicate good preservation during stages 2 and 4, providing evidence for well-oxygenated bottom waters.

A cessation of NADW production due to water-column stratification during the deglaciation between isotope stages 6 and 5e, and overall weaker deep-water circulation during stage 6 was proposed by Duplessy and Shackleton (1985) based on $\delta^{13}C$ benthic foraminifer data from 41 cores throughout the oceans. Distribution patterns of dark diamictons and their inferred palaeo-oceanographic settings, discussed in the previous sections, confirm Duplessy and Shackleton's (1985) findings. In addition, the dark lithofacies distribution provides a useful tool for the recognition of extensive glaciations when the continental ice sheets extended close to the shelf edge. Such situations appeared repetitively during stages 10 and 6, and at the stage 4/3 transition. Why has such a horizon not been detected at the stage 2/1 transition? One may argue that the advance of the continental ice sheets onto the shelf was less prominent. A perhaps more probable explanation is that a similar dark horizon has been deposited, but was subsequently overprinted by secondary oxidation as discussed in the previous section. The discovery of a dissolution peak ending in termination I_B (Henrich, 1986), the concentration of ice-rafted debris and occasional brownish to dark olive grey diagenetic laminations in the same levels may support the latter proposal.

Other questions deal with the palaeo-oceanography of the Norwegian–Greenland Sea during glacial extremes. Did a perennial sea-ice cover exist during stages 2 and 4 as proposed by Kellogg (1980), CLIMAP (1981) and Belanger (1982)? Intermediate carbonate shell production (Figs.13b–g), and good carbonate preservation during stages 2 and 4 (Fig.15), reflected by this study, seem to be inconsistent with a perennial ice cover. We propose seasonally changing environments, with an almost continuous ice pack in winter, and a more open packice interspersed with drifting icebergs during summer. Similar conclusions were drawn by Corliss et al. (1986) based on reinterpretation of Kellogg's (1980) data. The model proposed by Kellogg (1980) for the 82 ka situation is confirmed by the intermediate carbonate fluxes and low fluxes of ice-rafted debris determined in this study (Figs.13b–g). Good carbonate preservation (Fig.15) and the persistent occurrence of benthic foraminifers during stages 5d to 4 (Figs.5–8) suggest effective deep-water ventilation and exchange. Kellogg's (1980) model for the stage 5e circulation, and his finding that in earlier interglacials (i.e. stages 7 and 9) the influence of Atlantic waters was weaker is supported by the carbonate and ice-rafted debris flux data in this study (Figs.13b–g). The highest contents of subpolar planktonic foraminifers were observed during stage 5e (Fig.14). Intermittent to low values indicate the presence of Atlantic waters in the central sector of the Norwegian Sea during stage 7,

parts of stage 6 and 3, and in the lower part of stage 8.

Conclusions

Glacial–interglacial sedimentary cycles in the Norwegian Sea are revealed by a number of lithofacies which can be attributed to major palaeo-oceanographic changes. Characteristic dark lithofacies sequences are deposited during late glacial–early deglacial times. The most complete sequence of lithofacies below and at the glacial terminations reflects a low-salinity surface layer formed during the collapse of the marine-based parts of the continental ice sheets on the Norwegian shelf. Extensive reworking of organic matter-rich sediments during ice advance resulted in deep-sea deposition of terrigenous organic material during late glacial–early deglacial times. Decreased deep-water renewal and marine organic matter oxidation caused carbonate dissolution at the seafloor and, immediately after incipient burial, anoxic conditions within the sediments. Early interglacial conditions indicate a gradual decrease of ice rafting and a gradual re-establishment of carbonate production in surface waters. Well-oxygenated bottom waters cause early diagenetic oxidation of the upper part of the buried anoxic late glacial–early deglacial sediments and improved carbonate preservation. Less complete transitions without a return to fully oxygenated bottom waters characterize minor deglaciation horizons deposited during glacial periods, especially during stage 6.

Mapping of lithofacies distributions and late glacial–early deglacial sediment fluxes along an E–W transect across the Norwegian Sea shows a westward decrease in sediment supply. Late glacial–early deglacial sediment fluxes were high below the isotopic transitions and various phases within stage 6 during the past 350 ka. The most prominent source of terrigenous sediment in the investigated sector of the Norwegian Sea was the Scandinavian ice sheet. Additional transects across the Norwegian–Greenland Sea promise mass-balance calculations which could enable the differentiation of supplies of ice-rafted debris by the surrounding ice sheet and may enable estimates of the total ice volume of the Northern Hemisphere. Analysis of organic carbon fluxes and the composition of organic matter shows that land-derived organic matter or diagenetically altered fossil organic carbon is deposited in the deep Norwegian Sea basins at these times. A simultaneous rise of the CCD indicates that highly corrosive bottom waters were formed. Stable water-mass stratification might have inhibited deep-water renewal in the southeastern sector of the Norwegian Sea during these phases.

Good carbonate preservation over long glacial periods provides evidence that a year-round ice cover in the Norwegian–Greenland Sea is improbable. Seasonally changing conditions in sea-ice coverage must be assumed. Deep-water formation may not have been completely shut off during these periods but may have formed by mechanisms different from those occurring today.

Interglacial environments throughout the last 350 ka were strongly variable. The strength and circulation of the Norwegian Current during stage 5e best fit the modern conditions, while during stages 7 and 9 a considerably weaker Norwegian Current is detected. Influx of Atlantic waters into the eastern central sector of the Norwegian Sea is recorded during parts of stages 3, 6 and 8.

Acknowledgements

We thank captain Bruns and the crew of the new *Meteor* for their dedicated service during the first scientific cruise of this new research vessel into the Norwegian Sea in July 1986. Many colleagues from the joint scientific research project SFB 313 contributed with stimulating discussions. We offer special thanks to Claudia Henrich for assistance in preparing the final draft of the manuscript. Critical reviews from Drs. E. Jansen, S. Pfirmann and M. Sarnthein are gratefully acknowledged. We are indebted to Dr. H. Erlenkeuser at the ^{14}C Laboratory, University

of Kiel, for valuable help and advice at the automated carbonate preparation facility where samples were prepared for the Finnigan MAT 251 mass spectrometer. Dr. Leythäuser (KFA, Jülich) provided rock-eval data from core 23055, which is gratefully acknowledged. We thank U. Drechsler (carbonate and organic carbon measurements), A. Schröder, M. Stahlberg and J. Rust (handling of samples in the laboratory), U. Grützmacher, K. Lackschewitz, M. Ruff and C. Wieger (analysis of coarse-fraction components), Dr. D. Spiegler and A. Freiwald (preparation of planktonic foraminifers for SEM investigation), W. Reimann (operation of the SEM), U. Struck (drafting), and U. Schuldt (photographic assistance). This study was supported by grants from the German Research Foundation for the joint research project SFB 313 at Kiel University. A visit to Bergen University which enabled the first author to discuss data with colleagues is heartily acknowledged. This is publication 30 of the Special Research Project (SFB 313) at the University of Kiel.

References

Bard, E., Arnold, M., Duprat, J., Moyes, J. and Duplessy, J.C., 1987. Reconstruction of the last deglaciation: deconvolved records of $\delta^{18}O$ profiles, micropaleontological variations and accelerator mass spectrometric ^{14}C dating. Clim. Dyn., 1: 101–112.

Belanger, P.E., 1982. Paleoceanography of the Norwegian Sea during the past 130,000 yrs: coccolithophorid and foraminiferal data. Boreas, 11: 26–39.

Belanger, P.E. and Streeter, S.S., 1980. Distribution and ecology of benthic foraminifera in the Norwegian–Greenland Sea. Mar. Micropaleontol., 5: 401–428.

Berger, W.H., 1968. Planktonic foraminifera: selective dissolution and paleoclimatic interpretation. Deep-Sea Res., 15: 31–43.

Berger, W.H., 1982. Deglacial CO_2 buildup: Constraints on the coral reef model. Palaeogeogr., Palaeoclimatol., Palaeoecol., 40: 235–253.

Berger, W.H., 1971. Sedimentation of planktonic foraminifera. Mar. Geol., 11: 325–358.

Berger, W.H. and Vincent, E., 1986. Sporadic shutdown of North Atlantic deep water production during the Glacial–Holocene transition? Nature, 324: 53–55.

Boyle, E.A. and Keigwin, L.D., 1982. Deep circulation of the North Atlantic over the past 200,000 years: Geochemical evidence. Science, 218: 784–787.

Broecker, W.S., 1982. Ocean chemistry during glacial times. Geochim. Cosmochim. Acta, 46: 1689–1705.

CLIMAP, 1981. Maps of Northern and Southern Hemisphere Continental Ice, Sea Ice, and Sea Surface Temperatures in August for the Modern and the Last Glacial Maximum. (Geological Society of America Map and Chart Series MC-36.) Geol. Soc. Am., Boulder, Colo.

Corliss, B.H., Martinson, D.G., and Keffer, T., 1986. Late Quaternary deep-ocean circulation. Geol. Soc. Am. Bull., 97: 1106–1121.

Crowley, T.J., 1983. Calcium carbonate preservation patterns in the North Atlantic during the last 150,000 years. Mar. Geol., 51: 1–14.

Duplessy, J.C. and Shackleton, N.J., 1985. Response of global deep-water circulation to Earth's climatic change 135,000–107,000 years ago. Nature, 316: 500–507.

Duplessy, J.C., Arnold, M., Maurice, C., Bard, E., Duprat, F. and Moyes, F., 1986. Direct dating of the oxygen isotope record of the last deglaciation by ^{14}C accelerator mass spectrometry. Nature, 320: 350–352.

Eldholm, O., Thiede, J., Taylor, E. et al., 1987. Proc., Init. Reps. ODP 104, Part A.

Gerlach, S.A., Thiede, J., Graf, G. and Werner, F., 1986. Forschungsschriffahrt Meteor Reise 2 vom 19 Juni bis 16 Juli 1986. Ber. Sonderforschungsbereich Univ. Kiel, 313(4): 35–81.

Gorshkova, T.I., 1960. Sediments of the Norwegian Sea. In: Proc. Int. Geol. Congr., 21st, Colloq., 10, Submarine Geology. pp.16–22.

Hald, M. and Vorren, T.O., 1987. Stable isotope stratigraphy and paleoceanography during the last deglaciation on the continental shelf off Troms, Northern Norway. Paleoceanography, 2(6): 583–599.

Henrich, R., 1986. A calcite dissolution pulse in the Norwegian–Greenland Sea during the last deglaciation. Geol. Rundsch., 75(3): 805–827.

Henrich, R., 1989. Glacial/interglacial cycles in the Norwegian Sea: Sedimentology, paleoceanography and evolution of Late Pliocene to Quaternary Northern Hemisphere climate. In: O. Eldholm, J. Thiede et al., Proc. Final Reps. Ocean Drill. Proj. 104.

Henrich, R. and Wefer, G., 1986. Dissolution of biogenic carbonates: effects of skeletal structure. Mar. Geol., 70: 341–362.

Holtedahl, H., 1959. Geology and paleontology of Norwegian Sea bottom cores. J. Sediment. Petrol., 29: 16–29.

Hutson, W.H., 1980. Bioturbation of deep sea sediments: oxygen isotope and stratigraphic uncertainty. Geology, 8: 127–130.

Imbrie, J. and Kipp, N.G., 1971. A new micropaleontological method for quantitative paleoclimatology: Application to a late Pleistocene Caribbean core. In: K.K. Turekian (Editor), The Late Cenozoic Glacial Ages. Yale Univ. Press, pp.71–181.

Imbrie, J., Hays, J.D., Martinson, D.G., McIntyre, A., Mix, A.C., Morley, J.J., Pisias, N.G., Prell, W.L. and Shackleton, N.J., 1984. The orbital theory of Pleistocene climate: Support from a revised chronology of the marine $\delta^{18}0$ record. In: A.L. Berger et al. (Editors), Milankovitch and Climate. Reidel, Dordrecht, Part 1. pp.269–305.

Jansen, E. and Bjørklund, K., 1985. Surface ocean circula-

tion in the Norwegian Sea, 15,000 B.P. to present. Boreas, 14: 243–257.

Jansen, E. and Erlenkeuser, H., 1985. Ocean circulation in the Norwegian Sea during the last deglaciation: Isotopic evidence. Palaeogeogr., Palaeoclimatol., Palaeoecol., 49: 189–206.

Jansen, E., Sejrup, H.P., Ejaeran, T., Hald, M., Holtedahl, H. and Skarbo, O., 1983. Late Weichselian paleoceanography of the Southeastern Norwegian Sea. Nor. Geol. Tidsskr., 63: 117–146.

Jansen, E., Henrich, R., Bleil, U., Kringstad, L. and Slettemark, B., 1988. Paleoenvironmental changes in the Norwegian Sea and the Northeast Atlantic during the last 2.8 Ma.: ODP/DSDP Sites 610, 642, 643 and 644. Paleoceanography, 3(5): 563–581.

Johannessen, O.M., 1986. Brief overview of the physical oceanography. In: B.G. Hurdle, (Editor), The Nordic Seas. Springer, New York, pp.103–127

Kellogg, T.B., 1975. Late Quaternary climatic changes in the Norwegian–Greenland Sea. In: S.A. Bowling and G. Weller (Editors), Climate of the Arctic. Univ. Alaska, Fairbanks, pp.3–36.

Kellogg, T.B., 1976. Late Quaternary climatic changes: evidence from deep-sea cores of Norwegian and Greenland Seas. Geol. Soc. Am. Mem., 145: 77–110.

Kellogg, T.B., 1977. Paleoclimatology and paleo-oceanography of the Norwegian and Greenland Seas: the last 450,000 years. Mar. Micropaleontol., 2: 235–249.

Kellogg, T.B., 1980. Paleoclimatology and Paleoceanography of the Norwegian–Greenland Sea: Glacial-interglacial contrasts. Boreas, 9: 115–137.

Kellogg, T.B., Duplessy, J.C. and Shackleton, N.J., 1978. Planktonic foraminiferal and oxygen isotopic stratigraphy and paleoclimatology of Norwegian Sea deep-sea cores. Boreas, 7: 61–73.

Kennett, J. and Srinivasan, M.S., 1980. Surface ultrastructural variation in *Neogloboquandrina pachyderma* (Ehrenberg): phenotypic variation and phylogeny in the Late Cenozoic. Cushman Found. Spec. Publ., 19: 134–162.

King, L.H., Rokoengen, K. and Gunsleiksrud, T., 1987. Quaternary seismostratigraphy of the Mid Norwegian Shelf, 65°–67° 30'N—a till tongue stratigraphy. Inst. Kontinentasokkelunders. Publ. No. 114, 58 pp.

Kögler, F.C., 1963. Das Kastenlot. Meyniana, 13: 1–7.

Labeyrie, L.D. and Duplessy, J.C., 1985. Changes in the oceanic $^{13}C/^{14}C$ ratio during the last 140,000 years: High-latitude surface water records. Palaeogeogr., Palaeoclimatol., Palaeoecol., 50: 217–240.

Martinsson, D.G., Nicklas, G.P., Hays, J.D., Imbrie, J., Moore, T.C. and Shackleton, N.J., 1987. Age dating and the orbital theory of the ice ages: development of a high-resolution 0 to 300,000 years chronostratigraphy. Quat. Res., 27(1): 1–29.

Meincke, J., 1983. The modern current regime across the Greenland–Scotland Ridge. In: H.P. Bott, S. Saxov, M. Talwani and J. Thiede (Editors), Structure and Development of the Greenland–Scotland Ridge. (NATO Conference Series.) Plenum, New York, pp.637–650.

Mix, A. and Fairbanks, R.G., 1985. North Atlantic surface-ocean control of Pleistocene deep-ocean circulation. Earth Planet. Sci. Lett., 73: 231–243.

Molnia, B.F., 1983. Distal glacial–marine sedimentation: Abundance, composition, and distribution of North Atlantic Ocean Pleistocene ice-rafted sediment. In: B.F. Molnia (Editor), Glacial–Marine Sedimentation. Plenum, New York, pp.593–626.

Molma, B.T., 1983. Subarctic glacial-marine sedimentation: a model. In: B.T. Molma (Editor), Glacial–Marine Sedimentation. Plenum, New York, pp.95–144.

Mosby, H., 1968. Surrounding Seas. In: A. Sømme, Geography of Nordeu. J.W. Cappelens, Oslo, Map 7, pp.18–26.

Olausson, E., 1985. The glacial oceans. Palaeogeogr., Palaeoclimatol., Palaeoecol., 50: 291–301.

Pfirman, S.L. and Solheim, A., 1989. Subglacial meltwater discharge in the open-marine tidewater glacier environment: Observations from Nordaustlandet, Svalbard Archipelago. Mar. Geol., 86: 265–281 (this issue).

Powell, R.D., 1983. Glacial–marine sedimentation processes and lithofacies of temperate tidewater glaciers, Glacier Bay, Alaska. In: B.F. Molnia, (Editor), Glacial–Marine Sedimentation. Plenum, New York, pp.185–231.

Prell, W.L., Imbrie, J., Martinson, D.G., Morley, J.J., Pisias, N.G., Shackleton, N.J. and Streeter, H.F., 1986. Graphic correlation of oxygen isotope stratigraphy application to the Late Quaternary. Paleoceanography, 1: 137–162.

Ramm, M., 1988. A stratigraphic study of Late Quaternary sediments on the Vøring Plateau, eastern Norwegian Sea. Mar. Geol., 83: 159–191.

Reynolds, L.A. and Thunell, R.C., 1986. Seasonal production and morphologic variation of *Neogloboquadrina pachyderma* (Ehrenberg) in the northeast Pacific. Micropaleontology, 32: 1–18.

Ruddiman, W.F., 1977. Late Quaternary deposition of ice-rafted sand in the subpolar North Atlantic (lat 40° to 65°N.). Geol. Soc. Am. Bull., 88: 1813–1827.

Ruddiman, W.F. and Glover, L.K., 1975. Subpolar North Atlantic circulation at 9300 yr B.P.: faunal evidence. Quat. Res., 5: 361–389.

Ruddiman, W.F. and McIntyre, A., 1981. The North Atlantic Ocean during the last deglaciation. Palaeogeogr., Palaeoclimatol., Palaeoecol., 35: 145–214.

Sarnthein, M., 1971. Surface sediments in the Persian Gulf and in the Gulf of Oman. II. Quantitative component analysis of the coarse fraction. "Meteor" Forschungsergeb., Reihe C, 5: 113 pp.

Sarnthein, M., Winn, K., Duplessy, J.C. and Fontugne, M., 1988. Global variations of surface ocean productivity in low and mid latitudes: influence of CO_2 reservoirs of the deep ocean and atmosphere during the last 21,000 years. Paleoceanography, 3(3): 361–399.

Sarynina, R.N., 1972. Conditions of origin of cold deep-sea waters in the Bear Islands channel. In: A.J. Lee and H. Charnock (Editors), Proc. Symp. (Dublin, 25–27 September, 1969). Int. Counc. Explor. Sea, Copenhagen.

Sejrup, H.P., Jansen, E., Erlenkeuser, H. and Holtedahl, H., 1984. New faunal and isotopic evidence on the Late Weichselian–Holocene oceanographic changes in the Norwegian Sea. Quat. Res., 21: 74–84.

Shackleton, N.J., 1977. Carbon 13 in *Uvigerina*: Tropical rain forest history and the equatorial Pacific carbonate dissolution cycles. In: R.L.N. Anderson and A. Malahoff (Editors), The Fate of Fossil Fuel CO_2 in the Oceans. Plenum, New York, pp.401–427.

Shackleton, N.J. et al., 1984. Oxygen isotope calibration of the onset of ice-rafting and history of glaciation in the Northeast Atlantic. Nature 307: p.620.

Streeter, S.S., Belanger, P.E., Kellogg, T.B. and Duplessy, J.C., 1982. Late Pleistocene paleoceanography of the Norwegian–Greenland Sea: Benthic foraminiferal evidence. Quat. Res., 18: 72–90.

Swift, J.H., 1986. The Arctic waters. In: B.G. Hurdle (Editor), The Nordic Seas. Springer, New York, pp.129–153.

Thiede, J., Suess, E. and Müller, P.J., 1982. Late Quaternary fluxes of major sediment components to the sea floor at the Northwest African continental slope. In: U. Von Rad et al. (Editors), Geology of the Northwest African Continental Margin. Springer, Berlin, pp.605–631.

Thiede, J., Diesen, G.W., Knudsen, B.E. and Snare, T., 1986. Patterns of Cenozoic sedimentation in the Norwegian–Greenland Sea. Mar. Geol., 69: 323–352.

Vorren, T., Hald, M. and Thomsen, E., 1984. Quaternary sediments and environments on the continental shelf off Northern Norway. Mar. Geol., 57: 229–257.

Wohlfeil, K., 1982. Verbreitung, Herkunft und Bedeutung der Psephite des Seegebietes zwischen den Färoer und Island. "Meteor" Forschunsergeb., Reihe C, 36: 31–56.

Wohlfeil, K., 1983. Verteilung und Herkunft der Sedimente in Lotkernen von der Island–Faröer-Schwelle (Nordatlantik). Geol. Rundsch., 72(1): 137–165.

Worthington, L.V., 1970. The Norwegian Sea as a Mediterranean basin. Deep-Sea Res., 12: 667–676.